**Article:**
Stewart, N.J., Higano, N.S., Wucherpfennig, L. et al. (2025) Pulmonary MRI in newborns and children. Journal of Magnetic Resonance Imaging, 61 (5). pp. 2094-2115. ISSN: 1053-1807

https://doi.org/10.1002/jmri.29669

# Pulmonary MRI in Newborns and Children

Neil J. Stewart, PhD,[1,2*] Nara S. Higano, PhD,[3,4,5] Lena Wucherpfennig, MD,[6,7,8] Simon M.F. Triphan, PhD,[6,7,8] Amy Simmons, MPhys,[1] Laurie J. Smith, PhD,[1] Mark O. Wielpütz, MD,[6,7,8] Jason C. Woods, PhD,[3,4,5] and Jim M. Wild, PhD[1,2]

Lung MRI is an important tool in the assessment and monitoring of pediatric and neonatal lung disorders. MRI can provide both similar and complementary image contrast to computed tomography for imaging the lung macrostructure, and beyond this, a number of techniques have been developed for imaging the key functions of the lungs, namely ventilation, perfusion, and gas exchange, through the use of free-breathing proton and hyperpolarized gas MRI. Here, we review the state-of-the-art in MRI methods that have found utility in pediatric and neonatal lung imaging, the structural and physiological information that can be gleaned from such images, and strategies that have been developed to deal with respiratory (and cardiac) motion, and other technological challenges. The application of lung MRI in neonatal and pediatric lung conditions, in particular bronchopulmonary dysplasia, cystic fibrosis, and asthma, is reviewed, highlighting our collective experiences in the clinical translation of these methods and technology, and the key current and future potential avenues for clinical utility of this methodology.

**Evidence Level:** 2

**Technical Efficacy:** Stage 2

J. MAGN. RESON. IMAGING 2024.

MRI is becoming increasingly used for imaging the lungs of children and infants with respiratory conditions, where the risks associated with ionizing radiation are of primary concern. In recent years, lung MRI methods have matured, notably: $T_1$, $T_2$-weighted and contrast-enhanced perfusion sequences are used as part of clinical protocols for assessment of lung abnormalities in cystic fibrosis (CF)[1]; ultra-short echo time (UTE) $^1$H lung MRI now provides comparable quality to CT for structural imaging in fibrotic disease[2] and nodule detection[3]; inhaled hyperpolarized $^{129}$Xe MRI for assessment of lung function is used clinically in the UK in patients 5 years and above[4] and has recently been approved by the FDA for use in patients down to an age of 12 years.[5] A PubMed search for (MRI) AND ((lung) OR (pulmonary)) AND ((neonatal) OR (pediatric)) reveals that the number of articles published matching these criteria has increased dramatically over the last 20 years, with a ~10-fold increase between 2000 and 2021. Alongside this, novel treatments for several lung diseases that have made a significant impact on lung health are becoming more readily available to patients, and there is a need for safe methods for longitudinal monitoring of lung structure and function to accompany these often-expensive treatments. In particular, the advent of triple combination therapy for CF has transformed quality of life in those who are genetically eligible for it,[6] and biologics show dramatic suppression of asthma exacerbations.[7] Conventional MRI is very safe in children and can be repeated throughout childhood as a monitoring tool.[8] The Fleischner society recently published a position paper on the clinical status of lung MRI, recommending clinical use of $^1$H MRI in children with CF[9] and the European Respiratory Society (ERS) highlighted the potential importance of free-

View this article online at wileyonlinelibrary.com. DOI: 10.1002/jmri.29669

Received May 24, 2024, Accepted for publication Nov 12, 2024.

*Address reprint requests to: N.J.S., POLARIS Building, 18 Claremont Crescent, Sheffield S10 2TA, UK. E-mail: neil.stewart@sheffield.ac.uk

From the [1]POLARIS, Division of Clinical Medicine, School of Medicine & Population Health, Faculty of Health, The University of Sheffield, Sheffield, UK; [2]Insigneo Institute of In Silico Medicine, The University of Sheffield, Sheffield, UK; [3]Center for Pulmonary Imaging Research, Pulmonary Medicine and Radiology, Cincinnati Children's Hospital Medical Center, Cincinnati, Ohio, USA; [4]Department of Pediatrics, University of Cincinnati College of Medicine, Cincinnati, Ohio, USA; [5]Department of Radiology, Cincinnati Children's Hospital Medical Center, Cincinnati, Ohio, USA; [6]Department of Diagnostic and Interventional Radiology, University Hospital Heidelberg, Heidelberg, Germany; [7]Translational Lung Research Center Heidelberg (TLRC), German Center for Lung Research (DZL), Heidelberg, Germany; and [8]Department of Diagnostic and Interventional Radiology with Nuclear Medicine, Thoraxklinik at University Hospital Heidelberg, Heidelberg, Germany

breathing $^{1}$H lung MRI methods in bronchopulmonary dysplasia (BPD) assessment.[10]

There are several challenges in obtaining high quality MR images of the lung structure or function in children. The low proton density (20% ~ 40% of that of chest wall muscle[11]) and air-tissue susceptibility gradient driven short $T_2$* (~2 msec at 1.5 T, <1 msec at 3 T[12]) generally constrain $^{1}$H lung MRI, though a recent resurgence in diagnostic quality low-field MR ($T_2$* lung ~10 msec at 0.55 T[13]) is poised to overcome the latter. Dealing with motion—not only respiratory and cardiac, but also bulk motion of the subject, is of paramount importance in children. In adults, the normal range of respiratory rate is around 12–20 breaths per minute. Respiratory rates are higher in children and particularly rapid in infants; the median respiratory rate is approximately 44 breaths per minute at birth (up to 1 Hz in severe disease[14]) and 26 breaths per minute at 2 years old.[15] Rapid imaging during short breath-holds for compliant patients, or during free-breathing with respiratory gating and/or retrospective signal processing are critical, as are pre-exam communication with the patient, and techniques to minimize distress in the scanner—such as low acoustic noise sequences, A/V equipment for distraction etc.—to allow the exam to proceed without the use of sedation.

This review is structured in two parts:

i. an overview of the various MRI methods that have found utility in pediatric and neonatal lung MRI, with reference to the aspects of lung structure and function that they can probe, and how motion is dealt with,
ii. highlight of recent applications of these methods in children and neonates with lung disease, with a particular focus on the most-widely studied diseases to date, namely BPD and CF.

While other relatively recent reviews have been published focusing on either school-aged children or neonates.[16,17] However, there is a need for a comprehensive analysis of neonates, pre-school, and school-aged children to address the similarities and differences in MRI studies of these populations.

## Methods for Pulmonary MRI in Newborns and Children

### $T_1$-, $T_2$-Weighted

Fast gradient echo and spin echo sequences are common constituents of pediatric chest MRI protocols,[18] due to their simplicity of implementation and feasibility to be acquired within short breath-holds suitable for children. 3D $T_1$-weighted gradient echo sequences are commonly used for lung volumetry,[19] and are feasible for ungated morphological imaging in infants.[20] In addition, such sequences can be performed dynamically to evaluate airway dynamics, eg, tracheobronchomalacia in children.[21] Rapid, balanced steady-state free precession (bSSFP) sequences with their mixed $T_1$–$T_2$ contrast are a widely used in cardiovascular imaging, and in the lungs provide strong contrast between blood vessels and lung parenchyma.[22,23] Despite their relatively long echo times with respect to the short $T_2$* in the lung, $T_1$ and proton-density weighted spin echo sequences can also provide information about pathological water content, eg, as demonstrated in the lungs of preterm infants.[24,25] Fast spin echo approaches, in particular half-Fourier single-shot turbo spin echo (HASTE), provide good contrast of the parenchyma[26] and are suitable for breath-hold morphological assessment[27] and detection of infiltrates.[28] While $T_2$-weighted spin-echo sequences are generally sensitive to "plus pathologies" such as inflammation, fibrosis, atelectasis, mucus plugging, short-TE gradient echo sequences with $T_1$ or proton density contrast can provide sensitivity to "minus pathologies," eg, alveolar simplification, cysts, air trapping. Example $T_1$- and $T_2$-weighted images obtained from infants and children with CF (0–5 years) are shown in Fig. 1. The increased robustness to motion provided by non-Cartesian acquisition methods such as Periodically Rotated Overlapping ParallEL Lines with Enhanced Reconstruction (PROPELLER) makes them attractive for applications in infants and non-compliant children. Typically $T_2$-weighted, PROPELLER offers comparable contrast to HASTE sequences, and can be tailored to increase proton-density contrast; this has been utilized to assess CF lung disease in children and adolescents though with lower sensitivity than CT.[29]

### Contrast-Enhanced Imaging

Dynamic contrast-enhanced (DCE) MRI is a straightforward and easy-to-implement technique for imaging lung perfusion. Contrast agents are typically gadolinium-based with a safety profile that has been well studied in infants and children.[30] Rapid 3D gradient echo based $T_1$-weighted acquisitions—with parallel imaging, segmented k-space acquisition with view sharing (eg, Reference 31) and/or compressed sensing[32] for maximal temporal resolution—allow the visualization of an intravenously injected contrast bolus as it circulates through the pulmonary arterial system, the left heart, the aorta, and the bronchial circulation. DCE perfusion acquisitions are included within pediatric protocols used clinically in some centers for assessment of CF[33] and congenital lung malformations,[34] though adoption of DCE methods in children is not widespread at present. Assessment of the necessity of DCE MRI in pediatric lung disease in light of evidence of gadolinium deposition[35] is likely to vary by center/country and the clinical question at hand. Example images acquired from infants and children with CF (0–5 years) are shown in Fig. 1.

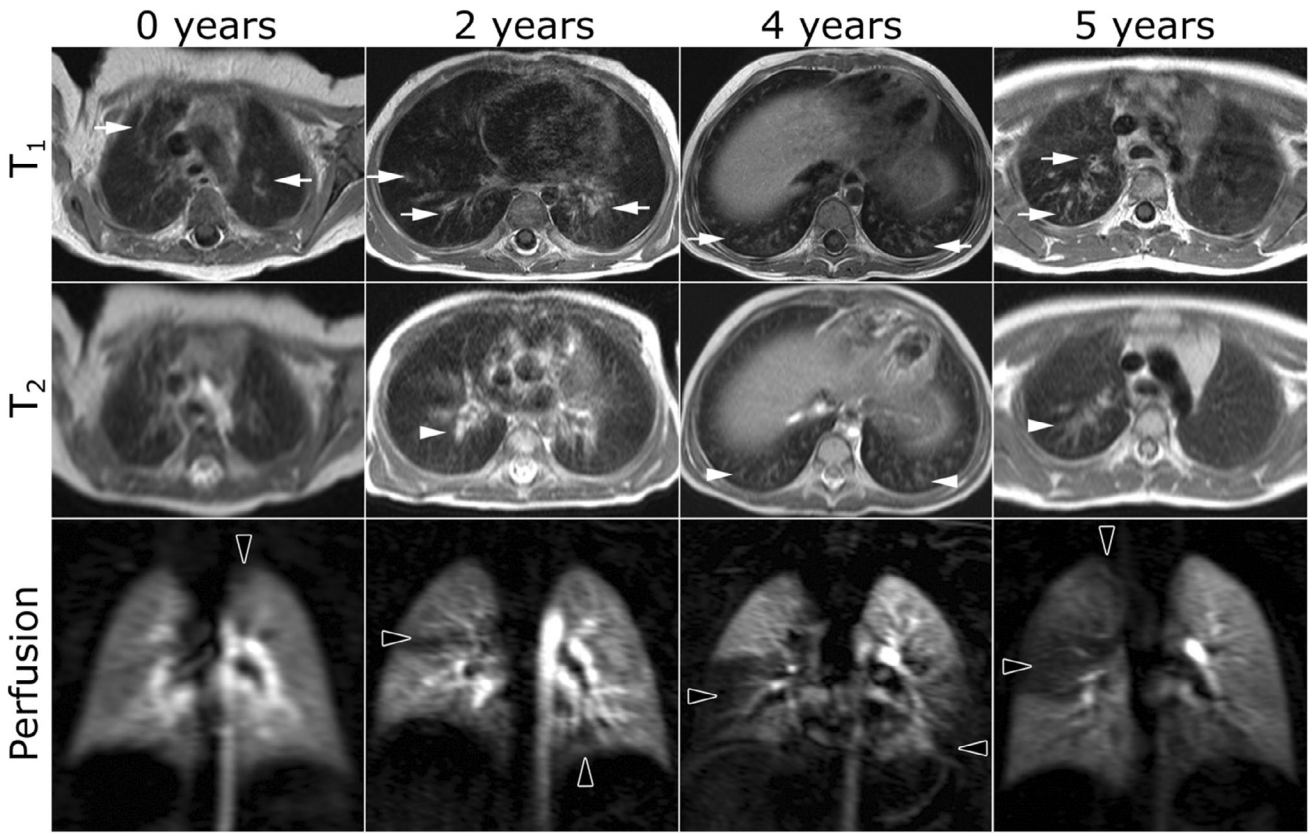


**FIGURE 1: Structural $T_1$-weighted gradient echo and $T_2$-weighted (HASTE) imaging alongside gadolinium contrast enhanced perfusion imaging in infants and children 0–5 years old with cystic fibrosis. Reprinted with permission of the American Thoracic Society.[1] Copyright © 2024 American Thoracic Society. All rights reserved. The American Journal of Respiratory and Critical Care Medicine is an official journal of the American Thoracic Society. White arrows: airway structural abnormalities including wall thickening and/or bronchiectasis, white arrowheads: mucus plugging, black arrowheads: perfusion abnormalities. HASTE = half-Fourier single-shot turbo spin echo.**

### *Non-Cartesian Acquisitions & Ultra-Short/Zero Echo Time*

Non-Cartesian (radial, spiral etc.) acquisitions with center-out k-space read-outs can counteract the rapid $T_2$* decay of proton signal in the lung tissue, providing improved signal-to-noise. An optimized 3D radial UTE acquisition with variable-density read-out and coarse 3D slab selection has been developed[36] and implemented in a number of sites for adult and pediatric lung imaging, providing improved proton-density weighting with preserved signal in lung parenchyma compared with conventional gradient echo methods. The long scan times of 3D radial UTE approaches necessitate acquisition during quiescent breathing in combination with some form of respiratory gating (prospective or retrospective), and with a pseudorandomized view order to allow for reconstruction with an arbitrary subset of acquired data. Respiratory bellows can be used in older children but present challenges in infants[14]; center-out acquisitions inherently repeatedly sample $k_0$, which provides an alternative "self-navigated" motion tracking waveform, allowing for retrospective discarding of data corrupted by bulk motion and reconstruction of images with reduced motion artifact. The 3D radial approach has been adapted for neonates to provide high spatial resolution (~0.7 $mm^3$) and full chest coverage in non-sedated, tidal-breathing infants with and without lung disease,[37] and in a follow-up study, the proton-density-weighted UTE lung intensity was found to be regionally associated with CT lung density in infants with a wide range of normal and pathological lung densities.[38] While 3D radial performance is generally high in infants and children, the long acquisition times (~5 to 15 minutes depending on FOV) are not ideal for rapid clinical throughput, and alternatives have been explored. Pseudo-3D stack-of-spirals methods have been used (predominantly on Siemens systems) to greatly reduce the acquisition time at the expensive of susceptibility to motion artifacts[39]; such approaches may even be feasible at breath-hold for resolutions ≥2 $mm^3$ in compliant children.[40] In addition, Fermat-looped, orthogonally encoded trajectories (FLORET)[41] (primarily developed on Philips systems), can offer significantly reduced scan times (~25%–40% that of 3D radial), while preserving image quality, resolution, and retrospective gating capabilities. The feasibility of FLORET

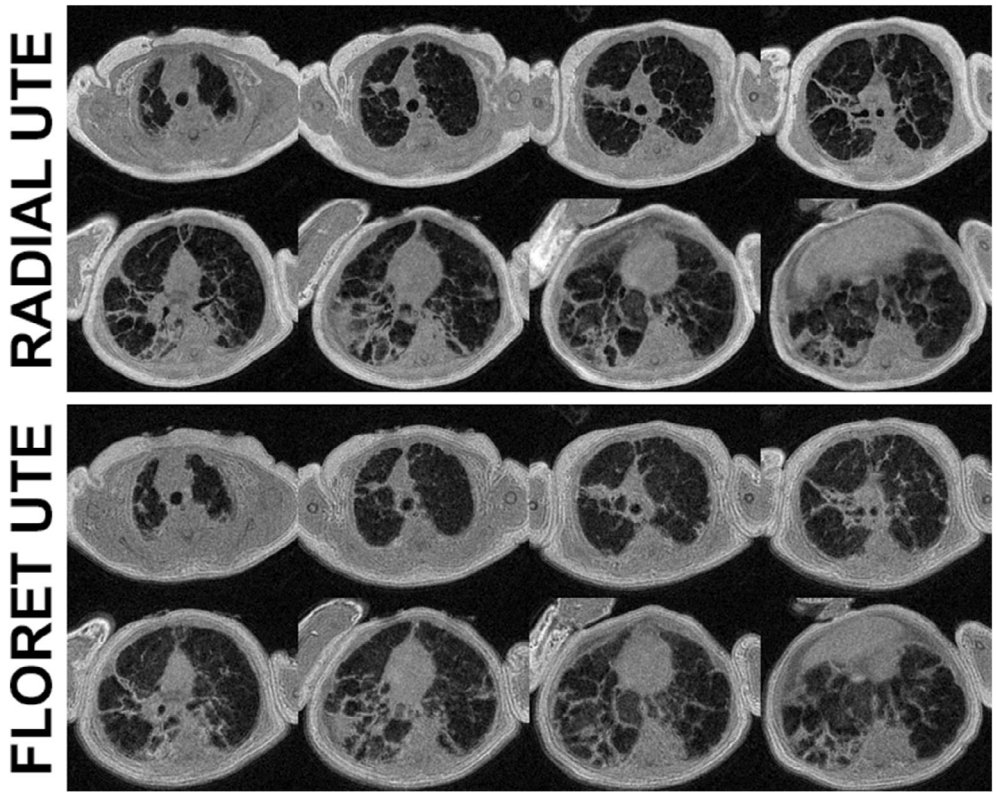


**FIGURE 2: Comparison of UTE structural lung images acquired with 3D radial and FLORET trajectories in a neonate with bronchopulmonary dysplasia. Both images were acquired with 180 $mm^3$ FOV and 0.7 mm isotropic resolution. Scan time was 16 minutes 44 sec for 3D radial UTE and 4 minutes 41 sec for FLORET UTE. (Images provided courtesy of Professor Sean Fain and Dr Andrew Hahn at University of Iowa.) FLORET = fermat-looped, orthogonally encoded trajectories; FOV = field of view; UTE = ultrashort echo time.**

has been investigated in pediatric subjects with CF,[42] and is under ongoing study in pre-term infants (Fig. 2).[43]

Zero echo time (ZTE) methods—in which the spatial encoding gradients are switched on at the time of the radiofrequency pulse excitation—show promise for structural lung imaging,[44] having similar contrast to UTE, and can be acquired during free-breathing with retrospective gating to investigate lung function.[45] The low acoustic noise footprint of these sequences is attractive for pediatric and especially neonatal applications to improve compliance and patient comfort, for example reducing the chance of subjects awakening when imaging during asleep, however such sequences are yet to show the same diagnostic performance as UTE.[46]

Beyond retrospective respiratory gating to reconstruct images at end expiration, continuous acquisition of 3D UTE data throughout the breathing cycle allows for reconstruction at various inflation states. Tidal volumes can be calculated from images reconstructed at end expiration and inspiration, and agreement between such UTE-measured tidal volumes and those predicted by physiologic scaling has been reported in neonates.[14] Furthermore, after registering images to a reference respiratory state, signal intensity differences between respiratory state images can be compared to calculate the fractional ventilation—a measure of ventilation akin to that measured by hyperpolarized gas MRI and PREFUL as discussed in the following subsections, and a subject of ongoing research.[39,47] In recent years, a wealth of motion-compensated/motion-resolved image reconstruction techniques have been proposed to improve the quality of retrospectively gated reconstructions. XD-GRASP incorporates respiratory motion as an additional regularization term into an iterative compressed sensing reconstruction,[48] while Zhu et al proposed an iterative motion compensation (iMoCo) strategy that instead incorporates motion fields from image registration of respiratory-motion-resolved UTE images into the CS algorithm.[49] iMoCo UTE images in pediatric and infant patients (Fig. 3) demonstrated clear pulmonary structures, and both higher apparent SNR and CNR compared to other motion correction strategies. A challenge of the multi-step iMoCo strategy is its dependence on image quality at each post-processing step. To address this, Zou et al introduced motion-compensated smoothness regularization on manifolds (MoCo-SToRM),[50] an unsupervised deep-learning scheme for MoCo reconstruction for application in free-breathing lung MRI. This study experimentally demonstrated improved structural resolution with MoCo-SToRM compared with iMoCo and XD-GRASP in four adults and one infant with BPD, with improvement particularly pronounced when

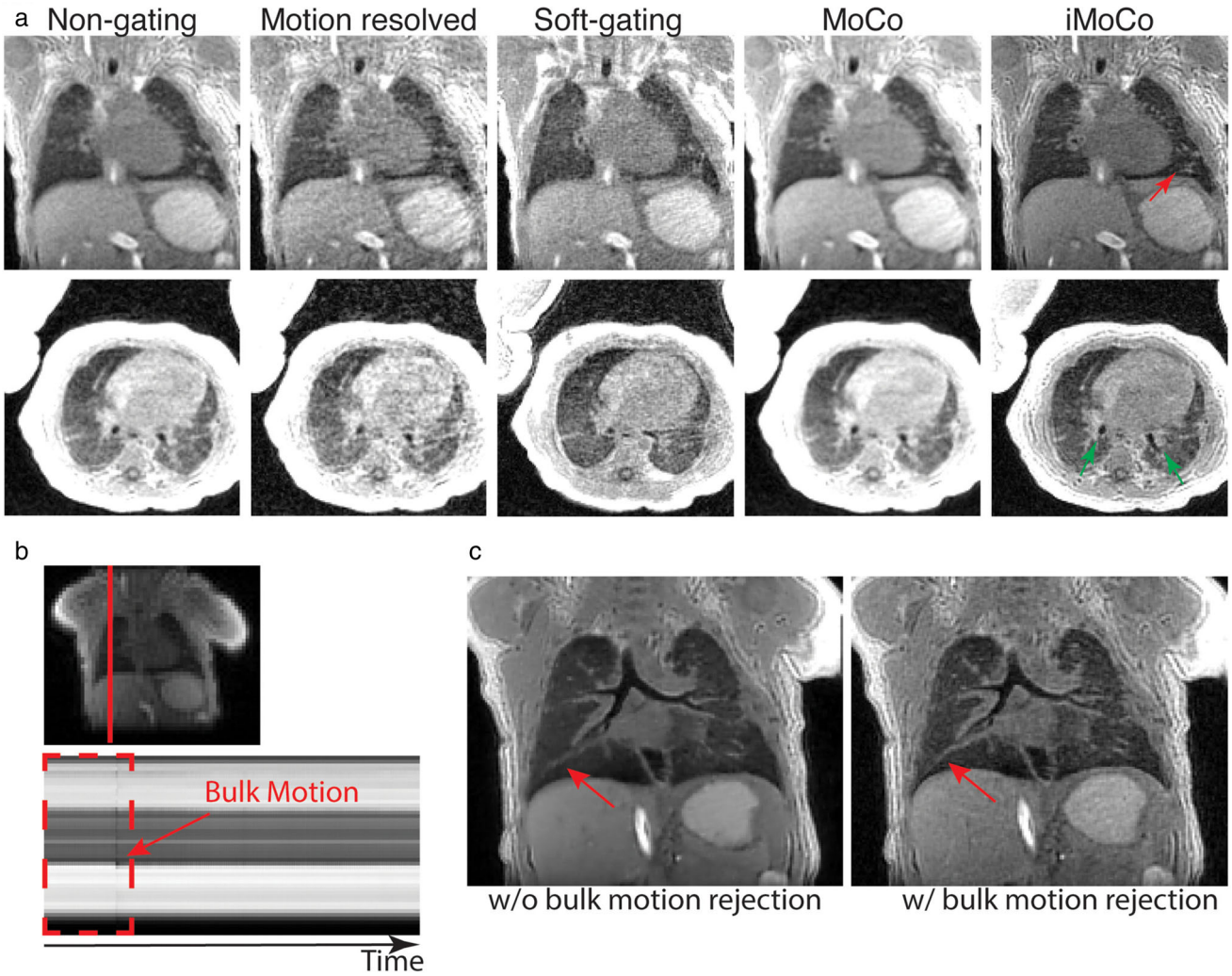


**FIGURE 3: (a) Illustration of improved motion compensation and signal-to-noise ratio of iterative motion compensation (iMoCo) reconstruction compared with non-gated, XD-GRASP-like motion-resolved, soft-gated reconstructions, and non-iterative motion compensated (MoCo) reconstructions in a 10-week-old infant. Reprinted with permission from Reference 49. Red arrows indicate vessels and green arrows the airways visualized on the iMoCo images. (b) Image-based motion navigator, iMoCo images without (c) and with (d) bulk motion rejection showed reduced motion blurring after bulk motion compensation. (Data highlighted by the red-dash rectangle were removed prior to reconstruction as they were acquired prior to a bulk movement; red arrow.) XD-GRASP = extra-dimensional golden-angle radial sparse parallel.**

a scan was corrupted by multiple bulk motion events. Most recently, motion-compensated low-rank reconstruction (MoCoLoR) has been developed to add a further low-rank constraint on the motion fields, and has ventilation mapping with both signal intensity based and deformation field-based methods has been reported.[51]

A technique combining highly undersampled 2D radial or 3D stack-of-stars methods with rapid, serial image reconstruction—dubbed "real-time MRI"[52]—has recently shown promise for volumetric coverage of the chest in children on a time scale of the order of tens of seconds with high robustness to respiratory motion.[53] This approach is currently limited by the requirement for a custom reconstruction set-up with dedicated multi-GPU machine for real-time reconstruction, but if demonstrated to be scalable, could help dramatically reduce the duration of high-resolution scans for morphological lung MRI exams.

### *Inhaled Hyperpolarized Gas Imaging*

Hyperpolarized gas MRI has matured into an important modality for imaging the function and microstructure of the lung.[4] While several of the landmark studies referenced herein have been performed using $^{3}$He gas, its heavily restricted availability and high cost have moved the field toward $^{129}$Xe gas over the last 5 to 10 years; moreover, $^{129}$Xe offers additional functionality with its ability to probe gas exchange function. The key aspects of lung function accessible with hyperpolarized gas MRI and the methods used in each case are described briefly here. For further details, we refer the reader to protocol reference paper published by the $^{129}$Xe

MRI Clinical Trials Consortium (note: these protocols are recommended for imaging of adult subjects).[54]

*VENTILATION.* 2D/3D gradient echo imaging during a short breath-hold after inhalation of a dose of hyperpolarized gas can be used to visualize the gas delivery to the lungs and its distribution, i.e., the lung ventilation and its heterogeneity. Beyond qualitative assessment, ventilation abnormality is most-commonly quantified by the ventilation defect percentage (VDP); the percentage of lung that yields no signal, i.e., is not ventilated. Ventilation heterogeneity can further be quantified by histogram analysis and the coefficient of variation of ventilated signal[55] and images can be presented as maps colored by binning the signal according to a healthy reference distribution.[56] In addition, imaging can be performed repeatedly to study ventilation *dynamics* and derive maps of the gas turnover per breath known as fractional ventilation.[57] This has been shown to be feasible in pediatric participants[58] and provide regional information comparable to the global information obtained from the multi-breath washout pulmonary function test—a sensitive marker of ventilation heterogeneity.

*MICROSTRUCTURE.* Diffusion-weighted imaging of hyperpolarized gases is feasible by inserting bi-polar diffusion gradients of modest strength into a spoiled gradient echo sequence. The apparent diffusion coefficient (ADC) of hyperpolarized gases in the lungs is reduced due to restriction by the alveolar walls; a two *b*-value measurement of ADC therefore provides a simple metric of alveolar size that is highly sensitive to, eg, emphysematous tissue destruction.[59] Diffusion in the lungs is known to be non-mono-exponential in nature, and multiple (>2) *b*-value diffusion-weighted imaging of hyperpolarized gases has been explored to better model the signal behavior and relate it to microstructural parameters. Notably, the cylinder model which treats the airways as cylinders and introduces two orthogonal diffusion coefficients,[60] and the stretched exponential model which introduces a diffusion heterogeneity index.[61] The application of these models is compared in patients with obstructive and restrictive lung diseases in Chan et al.[62]

*GAS EXCHANGE.* Upon inhalation, xenon partially dissolves in the lung parenchyma and pulmonary capillaries; $^{129}$Xe exhibits discrete chemical shifts in the parenchyma and blood plasma (collectively "membrane") and the red blood cells, approximately 200 ppm downfield from the resonance of $^{129}$Xe gas in the alveoli. Information about gas exchange—a key function of the lung—can be obtained from the $^{129}$Xe signals in these different environments by $^{129}$Xe MR spectroscopy.[63] Time-resolved spectroscopy and modeling of $^{129}$Xe uptake in the membrane and red blood cells using chemical shift saturation recovery can provide quantitative measures of lung microstructure and function.[64,65] Spatial localization can be achieved through chemical shift imaging techniques, typically 3D UTE radial in design to overcome the short 1–2 msec $T_2$* of dissolved $^{129}$Xe, with chemical shift separation according to the 1-point Dixon, whereby the echo time is chosen to induce a 90° phase difference between M and RBC resonances,[66] or using multi-echo approaches with matrix inversion[67] or IDEAL decomposition.[68]

Quantitative assessment of pathological changes in hyperpolarized gas MRI metrics often involves comparison with a reference age-matched healthy cohort. Recently, efforts have been made to establish such reference distributions for $^{129}$Xe MRI gas exchange metrics in healthy children,[69] and study their variation with age.[70] In the future, the use of predicted metric values may be envisaged in the same manner as that of pulmonary function tests.[71]

The doses used for $^{129}$Xe MRI—typically ≤1 L—and short breath-hold procedure are safe and well below the threshold required to induce anesthesia.[72] Walkup et al reported 100% tolerability and no serious or severe adverse events associated with xenon inhalation in children aged 6–16 years (including healthy control subjects and participants with CF).[73] As is observed in adults, a decrease in $SpO_2$ ~6% was observed in most children, and some children experienced mild side effects such as dizziness, euphoria; all of which resolved quickly after the inhalation.[73] There is little safety data in children under the age of 5–6 years old, aside from a report on the feasibility of $^{129}$Xe MRI in premature newborns with BPD, wherein a similar transient $SpO_2$ decrease of ~4.5% was observed.[74]

It is worth noting that in recent years, perfluorinated gases have shown some promise as inhaled MR contrast agents for imaging lung ventilation and microstructure.[75] While not as sensitive and technologically mature as $^{129}$Xe lung imaging at present, $^{19}$F lung MRI has several advantages; no hyperpolarization requirement, short $T_1$ and can be imaged rapidly over multiple breaths and averaged to provide reasonable SNR,[76] similar gyromagnetic ratio to $^{1}$H reducing the need for specialized RF coils. A preliminary report suggests this method may be feasible in children.[77]

### Non-Contrast $^{1}$H MRI Ventilation & Perfusion: Fourier Decomposition, PREFUL & OE-MRI

Rapid (>3 frames/sec), repeated acquisition of balanced/spoiled gradient echo images during free-breathing, subject to spatial co-registration, yields a series of images with temporal changes in parenchymal signal that are dependent on the position in the respiratory and cardiac cycles. Fourier decomposition is a means to separate this signal-time behavior according to the respiratory and cardiac frequencies and produce maps of ventilation and perfusion, respectively.[78] Over the last 10 years, several developments and variations on the original FD method have been developed. Notably,

SElf-gated Non-Contrast-Enhanced Functional Lung imaging (SENCEFUL)[79] adds the acquisition of a $k_0$/DC navigator to provide the respiratory/cardiac modulated signal, and matrix pencil (MP) decomposition has been proposed to improve the robustness of FD MRI for estimating respiratory and cardiac frequencies.[80] Most recently, phase-resolved functional lung (PREFUL) has been developed as an alternative approach to process the registered time-series of images to obtain full respiratory and cardiac cycle reconstruction and subsequent phase-based analyses.[81] Zanette et al have demonstrated the feasibility of the PREFUL approach to map regional ventilation and perfusion in healthy infants (Fig. 4).[82] While typically 2D methods are used for FD methods due to the high temporal resolution requirement, PREFUL has been recently extended to 3D using a stack-of-stars approach.[83]

Oxygen-enhanced MRI, which uses the $T_1$-shortening property of paramagnetic molecular oxygen presents an alternative, widely available contrast agent for assessment of pulmonary ventilation.[84] Aside from one successful demonstration of $T_1$ mapping under different hyperoxic conditions in a study that included adolescents and young adults with CF,[85] this technique has had limited application in children. Clinical uptake has been further constrained by the relatively modest signal enhancement and the complication of multiple contributing physiological factors to the signal enhancement.

Take-home messages/Recommendations:

- Conventional $T_1$- and $T_2$-weighted sequences provide complementary contrast in the lungs to locally increased air, and fluid, respectively, characteristic of pathological features
- 3D UTE imaging is a non-ionizing alternative to CT
- DCE MRI is only used in a few centers in pediatrics, but substantial safety data is available
- PREFUL is the most widely applied of existing post-processing methods for mapping ventilation and perfusion from free-breathing $^1$H MRI
- Hyperpolarized $^{129}$Xe is a direct, sensitive measure of lung ventilation, and recent efforts to standardize $^{129}$Xe MRI metrics of gas exchange and their age-dependence should increase its utility in children
- Several recommended protocols have been published (eg, References 86,87), though most only include conventional $^1$H sequences. Niedbalski et al published a recommended protocol for hyperpolarized $^{129}$Xe lung imaging in adults.[54] We provide a table summarizing these approaches and when they should be used, alongside references for implementation (Table 1). For GE Healthcare scanners we provide a protocol on the web that can be filtered for pediatric cases (https://polaris-sheffield.github.io/sheffield-lung-protocol/).

## Applications of Pulmonary MRI in Newborns and Children

### *Lung Disease in Infants: Bronchopulmonary Dysplasia & Congenital Diaphragmatic Hernia*

In recent years, pulmonary MRI has found clinical and pathological relevance in infants, particularly in those born prematurely who have developed BPD, and those with congenital

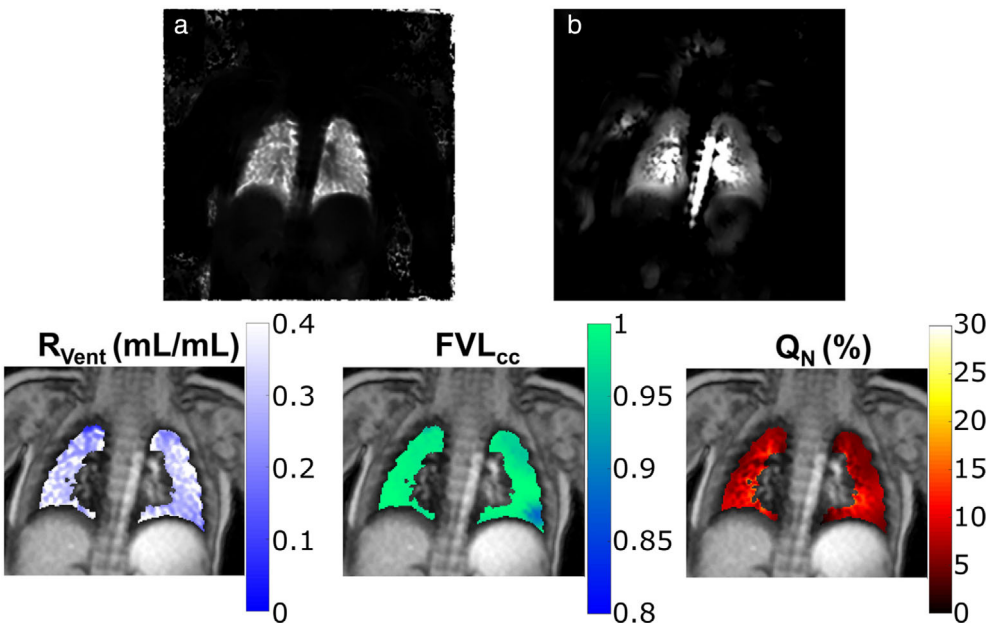


**FIGURE 4: PREFUL MRI results obtained from an 8-month-old infant using a 2D gradient echo sequence. Reprinted with permission from Reference 82. (a) Ventilation-, (b) perfusion-weighted maps. $R_{vent}$ = regional ventilation; $FVL_{cc}$ = flow-volume loop cross correlation; $Q_N$ = normalized perfusion percentage maps; PREFUL = phase-resolved functional lung.**

**TABLE 1. Suggested Pulse Sequences to Comprise a Pediatric Lung MRI Protocol**

| Sequence | Plane | Contrast | Indication | Usage/Comment | Breath-Hold* | Ref |
|---|---|---|---|---|---|---|
| ***$^{1}$H Structural*** | | | | ***Core components*** | | |
| 3D spoiled GRE[a] | Coronal | $T_1$/PD | Lung volume, air trapping | Optionally can be performed at RV to identify air trapping, and TLC | <10 s | 18,115 |
| 2D bSSFP[b] | Axial | $T_1$ & $T_2$ | Blood vessels, mucus, etc. | Optionally performed in free breathing where 50% slice overlap is recommended | <10 s or free-breathing | 22,86 |
| 3D UTE/ZTE | Axial/ Isotropic | PD | Alveolar simplification, cysts, air trapping, etc. | Product sequences not yet available for all vendors | Free-breathing (w/bellows/ self navigation) | 14,36 |
| 2D SSFSE[c] | Axial/ Coronal | $T_2$ | Inflammation, mucus plugging, etc. | Can be interchanged with PROPELLER | <10 s | 18,27 |
| PROPELLER[d] | Axial | $T_2$ | Inflammation, mucus plugging, etc. | Can be interchanged with 2D SSFSE | Free-breathing (w/navigator) | 29,108 |
| ***$^{1}$H Functional*** | | | | ***Optional/Local Preference*** | | |
| 2D/3D Fourier Decomposition | Coronal | | Ventilation & perfusion (2D only) | Spoiled/balanced GRE. Post-proc available on-line for Siemens only | Free-breathing | 140,168 |
| 3D dynamic SPGR with contrast[e] | Coronal | $T_1$ (w/contrast) | Perfusion | Recommended only for clinical queries re: perfusion deficit | ≤20 s breath-hold in older children or Free-breathing (w/bellows/self navigation) | 33 |
| ***$^{129}$Xe Functional*** | | | | ***Requires $^{129}$Xe polariser + multi-nuclear capable scanner*** | | |
| 2D SPGR/3D bSSFP | Coronal | Ventilation | 2D Cartesian implementation used in multi-site trials | | <10 s | 54,169 |
| 2D/3D DW SPGR | Coronal/ Axial | Alveolar airspace size | Recommended only for certain conditions (eg, BPD) | | Ideally <10 s but not yet widely achieved | 105,170 |
| 3D radial Dixon or multi-echo | Isotropic | Gas exchange | Recommended only for certain conditions (eg, ChILD, BPD) | | Ideally <10 s but not yet widely achieved | 70 |

[a]FLASH or VIBE (Siemens), SPGR (GE Healthcare), FFE (Philips).
[b]TrueFISP (Siemens), FIESTA (GE Healthcare), Balanced FFE (Philips).
[c]HASTE (Siemens), SSFSE (GE Healthcare), SSTSE (Philips).
[d]BLADE (Siemens), PROPELLER (GE Healthcare), MultiVane (Philips).
[e]With view-sharing, eg, TWIST or TWIST-VIBE (Siemens), TRICKS or DISCO (GE Healthcare), 4D-TRAK.
*Breath-holds are recommended for children aged 5 years and above.

disorders that affect pulmonary development (eg, congenital diaphragmatic hernia [CDH], pulmonary hypoplasia).

The most mature evaluations of lung structure in neonates have used reader-based scores. Higano et al implemented a scoring system modified from the Ochiai lung CT score[88] to assess high-resolution UTE images of lung structures in neonatal intensive care unit (NICU) inpatients with BPD.[89] This system evaluates pulmonary abnormalities including hyperexpansion, emphysema, fibrotic/linear opacities, mosaicism, bronchovascular bundle distortion, and subjective impression[20] (Table 2). In a cohort of 42 infants, MRI scores correlated significantly with BPD severity gradings, and furthermore, in multivariable modeling that also included several clinical parameters, MRI lung scores were the most significant predictor of the duration of any respiratory support, positive pressure support, and invasive ventilator support. This scoring scheme was then used with relevant clinical variables to create a binomial logistic regression to predict BPD patients' early risk of tracheostomy requirement[90]; the combined model performed better than models that only used MRI scores or clinical data. Förster et al devised a bespoke scoring system for $T_2$-weighted single-shot fast spin echo lung images (UNiforme Scoring of the disEAsed Lung in BPD, UNSEAL BPD[91]) (Fig. 5) that characterizes abnormalities including interstitial and airway remodeling, emphysematous changes, and ventilation inhomogeneity, with more emphasis on water content (eg, consolidation, bronchial wall edema, and mucus plugs) than with the modified Ochiai system for proton density-weighted images. The UNSEAL BPD score was able to identify infants with moderate and severe BPD disease grades, and structural changes present at term-age imaging that were specific to patients' gestational age at birth; the most premature infants presented with increased emphysema scores, while infants born after 26 weeks gestation had increased scores for interstitial enhancement, suggestive of fibroproliferative remodeling.

Beyond subjective reader scoring, more quantitative approaches are emerging to assess abnormal lung structures in infants, such as parametric mapping. Higano et al demonstrated proton-density mapping in infants with and without BPD and quantified the percentage of whole-lung tissue at abnormally high and low densities[92]; this percentage strongly correlated with clinical BPD severity levels and with relevant subscores from the modified Ochiai scoring system. Multi-echo UTE has been used to map $R_2$* as a novel measure of lung microstructure; in control infants a baseline was established for lung parenchymal $R_2$* at near term age of $335 \pm 65\ s^{-1}$, which was significantly lower than in healthy adults ($465 \pm 15\ s^{-1}$).[93] In a follow-up study, the $R_2$* in infants with BPD and ipsilateral CDH were found to be non-significantly higher than control infants, and $R_2$* in contralateral CDH was significantly higher.[94] The inverse relationship between tissue proton density and $R_2$* was influenced by the presence of disease, though with as-yet undetermined links to structural or physiological mechanisms.

Straightforward anatomical metrics have played an early but important role in understanding the asymmetric structural development and potential for pulmonary catch-up growth in infants with pulmonary hypoplasia, particularly CDH. Schopper et al measured prenatal and postnatal lung volumes using FSE and SPGR sequences in the ipsilateral and contralateral lungs of infants with left-sided CDH to investigate potential compensatory growth,[95] and found that lung volume grew faster in severe CDH compared with mild

**TABLE 2. Modified Ochiai Scoring Scheme for Features of Bronchopulmonary Dysplasia on Structural Lung MRI**

| | Scoring | | |
|---|---|---|---|
| **Feature** | **0** | **1** | **2** |
| 1. Hyperexpansion | None | Focal | Global |
| 2. Mosaic lung attenuation | None | Unclear | Obvious |
| 3. Emphysema, number of cysts/regions | None | Single | Multiple |
| 4. Emphysema, size | None | <5 mm | >5 mm |
| 5. Fibrous/interstitial, triangular subpleural opacities | None | 1–3 lobes | 4–6 lobes |
| 6. Distortion of bronchovascular bundles | Mild | Moderate | Severe |
| 7. Subjective impression | Mild | Moderate | Severe |
| *Maximal score* | 14 | | |

Scoring scheme taken from References 20,89. (See Reference 88 for example images depicting these pathological features.)

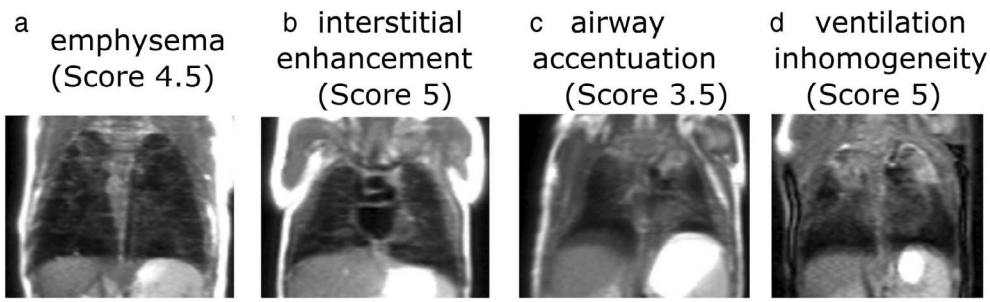


**FIGURE 5: Examples of HASTE images showing the key features of the UNiforme Scoring of the disEAsed Lung in bronchopulmonary dysplasia (UNSEAL BPD) scoring system. Reprinted with permission from Reference 91. Each feature is scored from 1 to 5 where 1 is absence and 5 is global high prevalence/severe disease. HASTE = half-Fourier single-shot turbo spin echo.**

CDH, and that total lung volume growth in moderate CDH was predominantly attributable to growth of the ipsilateral lung. To investigate whether this growth represented true parenchymal development or simply expansion of existing airspaces, Adaikalam et al used 3D UTE to measure normalized lung signal intensities and lung volumes, and calculated ipsilateral and contralateral lung mass in patients with CDH.[96] When compared to lung mass calculated from fetal MRI, the ipsilateral mass growth rate was higher than the contralateral rate, evidencing "catch-up" growth of lung mass in the more hypoplastic ipsilateral lung. Advancements in AI-based segmentation have made 3D lung volumetry a relatively trivial task; Mairhörmann et al recently reported that lung volumes and associated structural feature parameters derived from automated segmentations of HASTE images in premature babies were sensitive to BPD grade.[97] In particular, the lung elongation feature was found to be particularly complementary to conventional radiomic features.

Most approaches for assessing neonatal lung function rely on dynamic acquisition and reconstruction strategies that capture many lung inflation states. Using self-navigating 3D radial UTE in infants with severe BPD, Gouwens et al demonstrated that tidal volumes in cystic lung regions were higher than non-cystic regions, and that clinical ventilator settings for peak inspiratory pressure did not correlate with cystic tidal volumes.[98] Similar methods were used to generate end-expiratory and end-inspiratory gated UTE images in infants with BPD, showing that total lung volumes at functional residual capacity (FRC), tidal volumes, and minute ventilation were correlated with increasing severity grade.[99] Large total lung volumes (i.e., overinflation) were considered an imaging biomarker for small airways obstruction and air trapping. In a multi-center study, Katz et al used a breath-hold UTE sequence at expiration and inspiration to derive proton density measures that were sensitive to BPD grade in school-aged children born extremely pre-term.[100] Using PREFUL strategies as per,[82] Dyke et al showed regional variations in ventilatory function in preterm NICU inpatients and a significant difference in total VDP between groups of no BPD, BPD grade 0/1, or BPD grade 2/3.[101]

The feasibility of hyperpolarized gas lung ventilation imaging in infants between a few months and a few years of age was first shown by Altes et al[102] using $^{3}$He gas. Recently, the feasibility of short breath-hold $^{129}$Xe imaging for assessment of lung ventilation, microstructure and gas exchange in neonates with BPD has been reported,[74] providing preliminary evidence of significant ventilation defects and increased ADC indicating altered alveolar microstructure. The latter is in agreement with an ex-vivo study with hyperpolarized $^{3}$He, where dramatic alveolar remodeling and enlargement was observed in filamin-A deficiency—a disease with similar functional presentation to BPD,[103] and observations in later life as discussed below. Representative ventilation images obtained from Altes et al[102] and Stewart et al[74] are shown in Fig. 6.

BPD in infancy is known to cause lasting lung function deficiency later into childhood. Diffusion-weighted MRI using both hyperpolarized $^{3}$He[104] and $^{129}$Xe[105] gas has revealed increased ADC (reflective of increased alveolar size) in school-aged children with historic BPD-related pulmonary complications, indicating lung microstructural abnormalities post-infancy (Fig. 7). An earlier study using $^{3}$He MRI reported no difference in ADC between schoolchildren with historic BPD and term-born children,[106] however, the long diffusion times and non-imaging nature of the acquisition used were not ideal for measuring alveolar-restricted diffusion.[107] Furthermore, prematurity-related obstructive lung disease was found to be associated with increased ventilation abnormalities on hyperpolarized $^{129}$Xe MRI,[105] and both ventilation and perfusion abnormalities on $^{1}$H FD MRI[108] in childhood. Further studies of children born prematurely but without a historical diagnosis of BPD are warranted to investigate what insights about lung development and the impact of prematurity can be determined from hyperpolarized $^{129}$Xe diffusion-weighted MRI.[106,107,109]

### *Cystic Fibrosis*

The early detection and sensitive monitoring of lung disease in young children with CF are a prerequisite for optimized care and long-term outcomes.[110–113] Typical characteristics of

early CF lung disease are bronchiectasis, wall thickening and mucus plugging.[1,114] Since wall thickening and mucus plugging are accompanied by an increase in fluid and tissue a.k.a. "plus-pathologies," they can significantly improve the conditions for $^{1}$H MRI, and as such, even pathologies in the peripheral airways can be observed with a similar sensitivity to CT.[115,116] To date, several studies have demonstrated that chest MRI is sensitive to detect abnormalities in early CF lung disease.[1,117,118] While wall inflammation demonstrates an obvious contrast enhancement, mucus plugging is especially well visualized by MRI because of its high $T_2$ signal, but without contrast enhancement.[119] Also, bronchial air-fluid levels in sacculations and consolidations can also be visualized by a high $T_2$ signal due to the fluid content.[116] Pre- and post-contrast $T_1$-weighted imaging can provide complementary information by delineating mucus from the bronchial wall, as mucus does not exhibit enhancement post-contrast.[116] In addition to morphological abnormalities, $^{1}$H MRI can visualize perfusion abnormalities of CF lung disease with pulmonary DCE MRI. As a physiological response to airway obstruction and local hypoxia, delivery of blood to the affected lung region is downregulated (hypoxic pulmonary vasoconstriction).[120] Thus, perfusion imaging is an excellent tool to monitor functional impairment in CF.

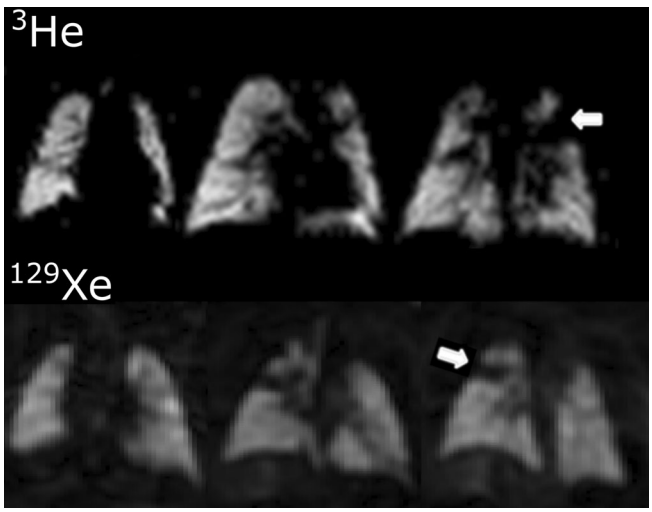


**FIGURE 6: Inhaled hyperpolarized gas images of lung ventilation in a 2-month-old infant using $^{3}$He (top)—reprinted with permission from Reference 102—and a 3-month-old infant using $^{129}$Xe (bottom)—reprinted with permission from Reference 74. Both infants were born prematurely, the latter with confirmed severe bronchopulmonary dysplasia. Arrows indicate major ventilation abnormalities.**

To quantify the pathologies detected by MRI, a chest MRI scoring system was introduced[33] that consists of a morphology score assessing structural changes (wall thickening/bronchiectasis, mucus plugging, sacculations/abscesses, consolidations; and special findings [mainly pleural reaction]), a perfusion score assessing perfusion abnormalities, and a global score (Table 3). The extent of disease is rated for each lobe as 0 (no abnormality), 1 (<50% of the lobe involved), or 2 (≥50% of the lobe involved). The MRI global score results from the sum of the morphology and perfusion score.

A prospective, longitudinal study in newborns and preschool children with CF (0–4 years, N = 96) demonstrated that MRI with this chest MRI scoring system is sensitive to detect the progression of early lung disease in preschool children with CF.[114] Moreover, structural lung abnormalities, especially bronchiectasis/wall thickening, detected by MRI were lower throughout infancy and preschool years when the CF diagnosis was established by newborn screening rather

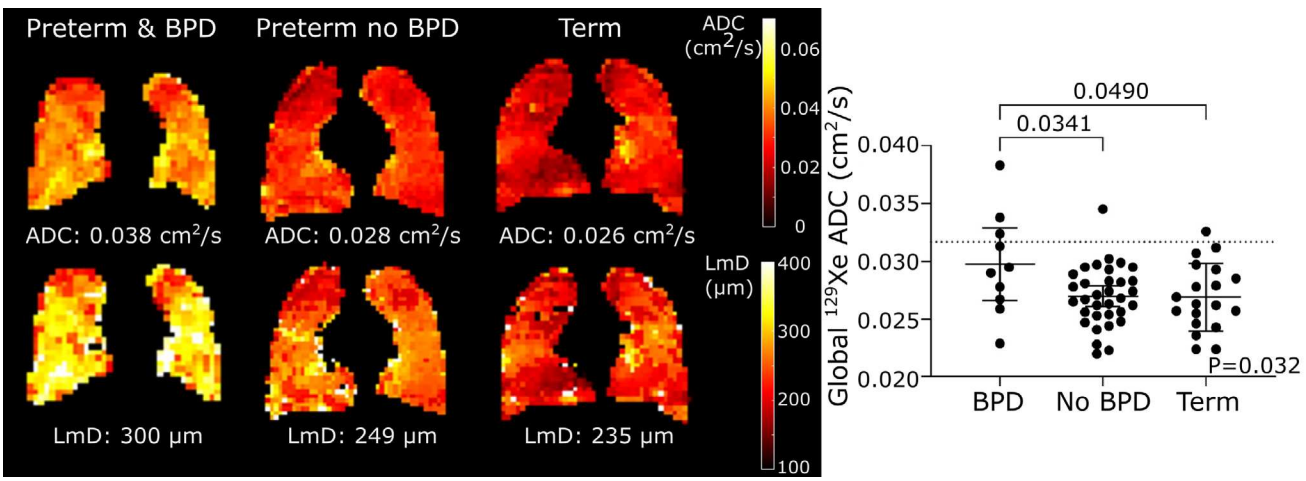


**FIGURE 7: $^{129}$Xe diffusion-weighted imaging in the lungs of school-aged children born prematurely with and without bronchopulmonary dysplasia (BPD). Reprinted with permission of the American Thoracic Society.[105] Copyright © 2024 American Thoracic Society. All rights reserved. The American Journal of Respiratory and Critical Care Medicine is an official journal of the American Thoracic Society. Left: apparent diffusion coefficient (ADC) and lung microstructural dimension (LmD) maps acquired from children born prematurely with and without BPD compared with term born children (global ADC and LmD are quoted). Right: distribution of $^{129}$Xe ADC values in the three groups showing elevated ADC in children born pre-term with BPD compared with those born prematurely without BPD and term born children.**

**TABLE 3. Scoring System for Morpho-Functional Lung MRI in Cystic Fibrosis**

| Feature | Right | | | Left | | | Maximal Feature/Global Score |
|---|---|---|---|---|---|---|---|
| | UL | ML | LL | UL | LG | LL | |
| 1. Bronchiectasis/wall thickening | /2 | /2 | /2 | /2 | /2 | /2 | /12 |
| 2. Mucus plugging | /2 | /2 | /2 | /2 | /2 | /2 | /12 |
| 3. Abscesses/sacculations | /2 | /2 | /2 | /2 | /2 | /2 | /12 |
| 4. Consolidation | /2 | /2 | /2 | /2 | /2 | /2 | /12 |
| 5. Special findings | /2 | /2 | /2 | /2 | /2 | /2 | /12 |
| 6. Perfusion size | /2 | /2 | /2 | /2 | /2 | /2 | /12 |
| *Maximal lobal/global score* | /12 | /12 | /12 | /12 | /12 | /12 | /72 |

Scoring scheme taken from Reference 33. Each feature is scored from 0 to 2 in each lobe where 0: absent, 1: present in <50% of the lobe, 2: present in >50% of the lobe. UL = upper lobe; ML = middle lobe; LL = lower lobe; LG = lingula.

than on the basis of clinical symptoms (Fig. 8). These findings demonstrate the importance of early diagnosis in CF to further delay or prevent lung damage in preschool children with CF.[114] Moreover, an association between the chest MRI score and potential risk factors for the early progression of CF lung disease such as respiratory symptoms, pulmonary exacerbations, anthropometry, and microbiology were found.[114] In addition to the ability of MRI and the corresponding scoring system for longitudinal diagnostic disease monitoring and detection of disease progression, MRI was found to be sensitive to depict response to antibiotic therapy and disease specific modulator therapy.[1,121,122]

In recent years, the feasibility of free-breathing Fourier Decomposition-based $^{1}$H MRI approaches in pediatric CF has been explored.[123,124] The original FD technique has been validated in adolescents and adults against DCE perfusion visually, and through reader scores,[125] and recently, in a multi-site study investigating response to triple combination therapy in children with CF and one or two F508del alleles, one site used PREFUL-based perfusion in place of contrast-enhanced perfusion to contribute to the aforementioned MRI score.[121] PREFUL-derived ventilation defect percentage was found to decrease after antibiotic treatment for pulmonary exacerbations in school-aged children with CF.[126] Similarly, free-breathing $^{1}$H MRI with matrix pencil based reconstruction has been used to visualize improvements in both lung ventilation and perfusion metrics in children with CF in response therapy including salbutamol inhalation[127] and triple combination therapy[128] (Fig. 9).

The assessment of regional ventilation obstruction in children with CF was first explored using dynamic $^{3}$He gas MRI[129] and since, hyperpolarized gas MRI ventilation metrics have been shown to correlate strongly with clinical measures including the lung clearance index from multi-breath washout test.[130,131] The high sensitivity of hyperpolarized gas MRI to subtle/minor abnormalities in lung ventilation have enabled the detection of sub-clinical airway obstruction—abnormal VDP where $FEV_1$ is normal—in pediatric patients with CF.[132,133] Furthermore, in longitudinal studies, metrics including VDP and ventilation heterogeneity were reported to reveal sub-clinical changes at 1- or 2-year follow-up[130,134] (Fig. 10a). A key use of this unmatched sensitivity is in the evaluation of therapeutical efficacy,[135] and this is of great clinical interest with the recent advent of triple combination therapies. In addition to more traditional therapies such as chest physical therapy[136] and exercise therapy,[137] strong responses in VDP to ivacaftor therapy in adults with CF[138] (Fig. 10b) and antibiotics in school-aged children with CF[139] have been reported.

Recently, $^{129}$Xe ventilation MRI has been used as the standard against which to compare $^{1}$H(PREFUL)-based MR ventilation metrics in pediatric CF. In a multi-site study, a strong coarse agreement between the two techniques has been observed with a variable level of intra-subject disagreement[140] (Fig. 11), while a separate study reported agreement in stable CF and disagreement in CF patients with exacerbations.[141] PREFUL and $^{129}$Xe MRI ventilation measures are reported to have similar repeatability in pediatric CF.[142] In addition, a multi-site analysis has been conducted to support the use of $^{129}$Xe ventilation MRI in multi-site drug trials, showing excellent agreement in VDP between analysts.[143]

### *Pediatric Asthma*

Asthma is a highly prevalent chronic respiratory disease characterized by airway inflammation and exacerbations. Most pulmonary MRI studies of asthma to date have focused on adult asthma, however, childhood asthma can present quite differently, and there is a particular need for a personalized

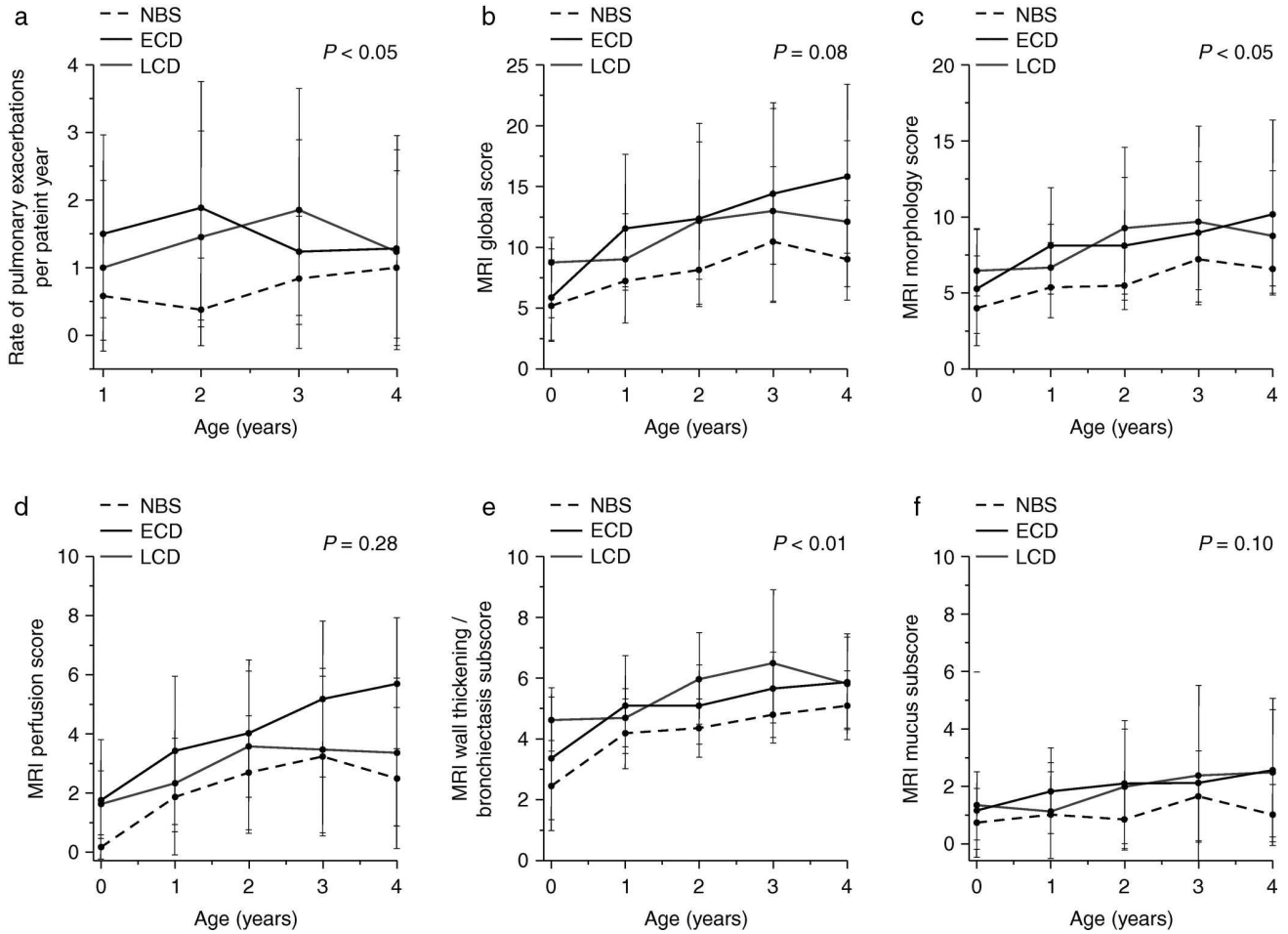


**FIGURE 8: Rate of pulmonary exacerbations (a) alongside the time-course of global (b), morphological (c), perfusion (d), wall-thickness/bronchiectasis (e) and mucus (f) MRI scores derived from the scoring system in Table 3 in infants and preschool children with cystic fibrosis over the first few years of life, stratified according to diagnosis method; new-born screening (NBS), early clinical diagnosis (ECD), late clinical diagnosis (LCD). Reprinted with permission of the American Thoracic Society.[114] Copyright © 2024 American Thoracic Society. All rights reserved. The American Journal of Respiratory and Critical Care Medicine is an official journal of the American Thoracic Society.**

management/treatment approach. In school-aged children with asthma, inhaled $^{3}$He MRI has been reported to be safe with minimal minor side effects (headache, dizziness).[144] Ventilation defects are heterogeneous in appearance,[145,146] and VDP has been found to correlate with clinical metrics including blood eosinophil count.[146] More recently, $^{129}$Xe MRI VDP has been shown to correlate with asthma severity and healthcare utilization,[147] and beyond severity staging, provides a sensitive means to assess bronchodilator response.[148] Lung MRI is anticipated to find utility in the assessment of novel biologic treatments for pediatric asthma in the immediate future.

### *Other Diseases*

Beyond BPD, CF, and asthma, several other diseases with associated pulmonary morbidity in children have been studied using lung MRI. Primary ciliary dyskinesia (PCD)—a genetic disorder of the cilia causing lung disease in children—shows comparable MRI structural features to CF.[149] Using matrix-pencil based structure–function imaging, Nyilas et al found considerable heterogeneity in ventilation and perfusion abnormality and poor correspondence of MRI measures with spirometry in children with PCD.[150] Single-site[151] and multi-site[152] studies with hyperpolarized $^{3}$He and $^{129}$Xe MRI, respectively, have similarly shown heterogeneity in the presentation of ventilation abnormalities in childhood PCD, and correlation between VDP and lung clearance index (Fig. 12). Willmering et al recently reported reduced $^{129}$Xe-MRI derived gas exchange function in pediatric patients after bone marrow transplantation and worsened ventilation heterogeneity in childhood interstitial lung disease (ChILD).[70] A preliminary study also indicate the similar structural features in ChILD that can be visualized on HASTE and PROPELLER images compared with clinical CT.[153] Moreover, the utility of $^{129}$Xe MRI in identifying airway obstruction following hematopoietic stem cell transplant (HSCT) in children has also been explored.[154] With approval for clinical use of $^{3}$He and $^{129}$Xe in Sheffield, UK, and the recent milestone

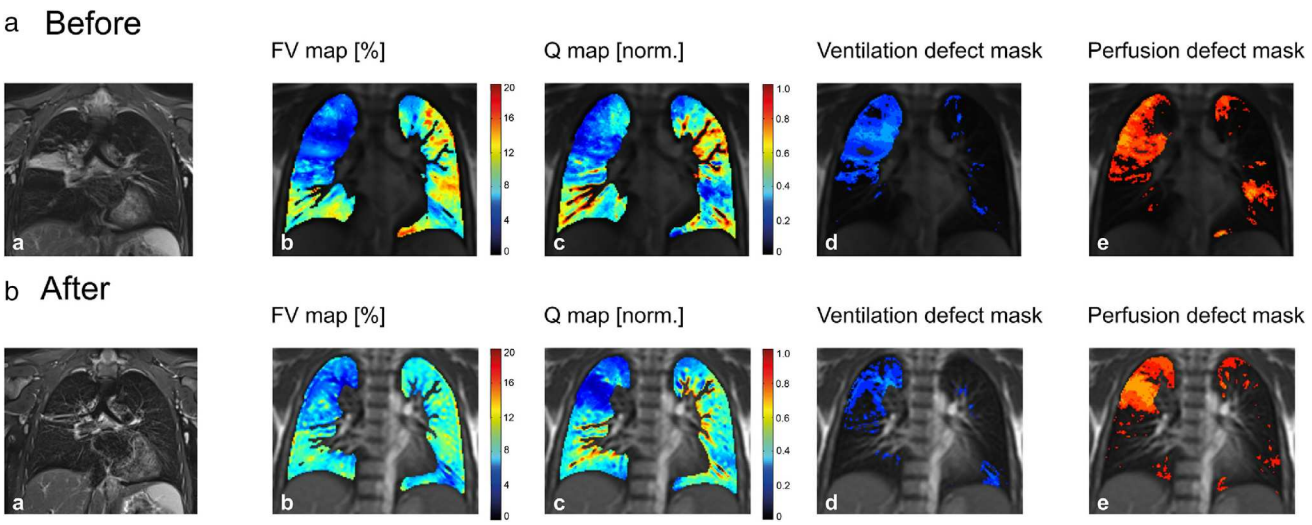


**FIGURE 9: Comparison of pulmonary MRI before and after triple combination therapy in an 11-year-old patient with cystic fibrosis. From left to right: morphological (PROPELLER) images, fractional ventilation (FV), perfusion (Q) and ventilation and perfusion defect masks derived from dynamic 2D bSSFP-based matrix pencil imaging, respectively before (a) and after (b) the therapy showed partial resolution of atelectasis in the right upper lobe and reduced bronchial wall thickening on morphological imaging, and corresponding improvement of ventilation and reduced ventilation-perfusion mismatch. Reprinted with permission from Reference 128. bSSFP = balanced steady-state free precession; PROPELLER = Periodically Rotated Overlapping ParallEL Lines with Enhanced Reconstruction.**

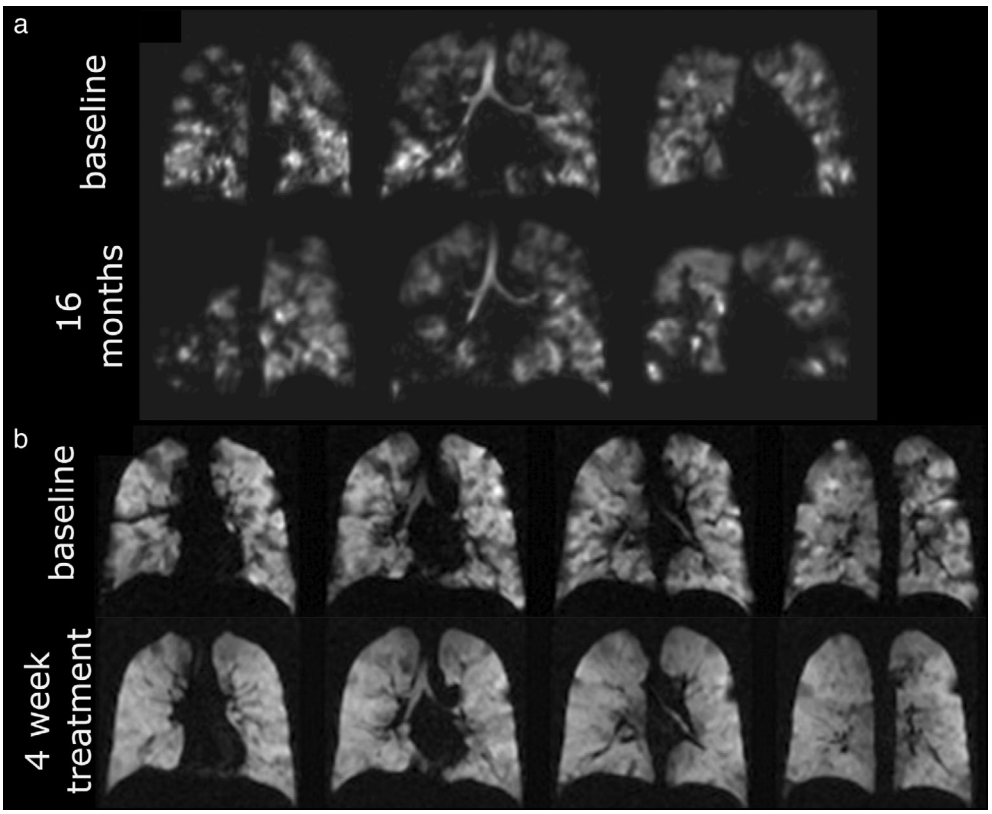


**FIGURE 10: (a) Worsening of ventilation heterogeneity (VDP change 16.6% to 27.3%) over 16 months while $FEV_1$ *z*-score and LCI did not change significantly in a pediatric patient with cystic fibrosis (CF) visualized by hyperpolarized $^3$He MRI.[134] (b) Dramatic improvement in ventilation in response to a 4 week course of ivacaftor treatment in an adult with CF visualized by hyperpolarized $^3$He MRI. Reprinted with permission from Reference 138. LCI = lung clearance index; $FEV_1$ = forced expiratory volume in 1 second; VDP = ventilation defect percentage.**

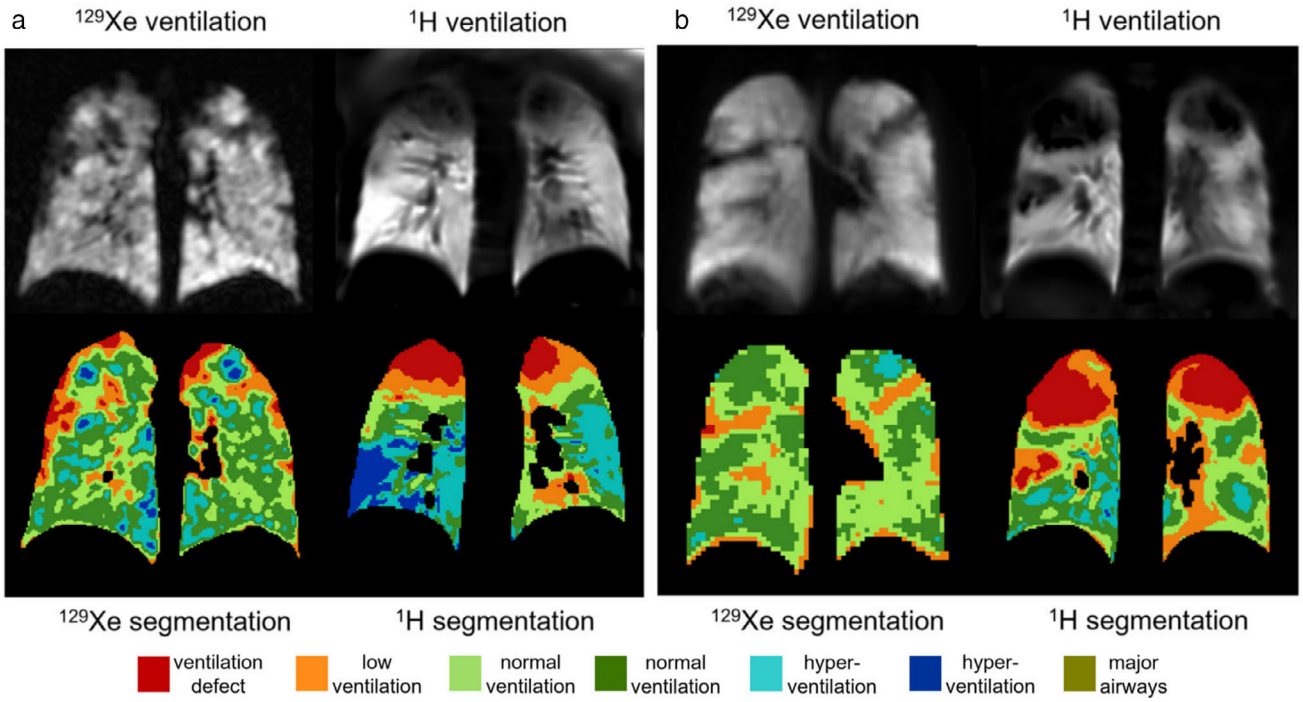


**FIGURE 11: Comparison of breath-hold $^{129}$Xe gas- and free-breathing $^{1}$H PREFUL-based ventilation maps in pediatric patients with CF, showing a variable level of agreement. Reprinted with permission from Reference 140. (a) Patient with mild CF (normal $FEV_1$) and (b) patient with moderate CF (abnormal $FEV_1$). PREFUL = phase-resolved functional lung; $FEV_1$ = forced expiratory volume in 1 second.**

FDA approval of $^{129}$Xe for ventilation imaging in patients 12 years and above, the utility of hyperpolarized gas MRI in older children in particular is set to expand. We have reported our experience of the impact of hyperpolarized gas MRI in clinical decision making in Sheffield in a recent review.[4]

Take-home messages/Recommendations:

- Free-breathing $^{1}$H UTE imaging may be used in a dedicated NICU-housed MRI set-up to inform treatment and management decision making in neonates with BPD
- In CF, $^{1}$H lung MRI is being used in place of chest x-ray and CT for first point structural assessment in many centers
- Hyperpolarized $^{129}$Xe ventilation imaging is sensitive to sub-clinical disease in pediatric CF
- Diffusion-weighted and gas-exchange imaging with $^{129}$Xe are scientifically interesting but require further evaluation in large pediatric cohorts to establish clinical utility
- Pre- and post-therapy lung MRI is set to play a key role in the short- and long-term assessment of novel therapies in pediatric CF and asthma

## Remaining Challenges

### *Breath-Holds/Sedation*

In our experience, children aged 5 years and above can achieve breath-holds of 5–10 seconds in duration, although this requires coaching by a lung physiologist or physician, which will limit the feasibility more widely. Below this age, free-breathing methods are the only feasible option. Sedation for MRI is safe and well tolerated,[155] however, if feasible, imaging without sedation is desirable to lessen the logistical burden of the scan. In infants up to around 6–9 months of age, the feed and swaddle technique allows imaging without sedation.[14] Between 1 and 4 scan success rates are more variable, although comparable to that of spirometry.[124] Some centers routinely perform lung MRI under sedation,[86] and this decision is likely to be made according to local/national guidelines. Recent progress in faster imaging, more sophisticated motion monitoring and correction are all poised to contribute to incrementally improved feasibility of non-sedation imaging in the near future.

### *Research/Work-in-Progress/Non-Vendor Proprietary Sequences/Software*

A number of the methods discussed in this article, including radial and spiral $^{1}$H UTE, are not yet commercially available as products from all the major MRI manufacturers; PREFUL processing of Fourier decomposition MRI requires either the purchase of a software licence or the expertise to implement such processing locally; multi-nuclear pulse sequences are not yet available on all vendors and/or are not optimized for $^{129}$Xe by default. Such "research" sequences/methods are currently limited to academic centers, in particular, those with strong research collaborations with the scanner vendors. While standard $^{1}$H MRI sequences currently provide a comprehensive structural assessment of the lungs, the field is

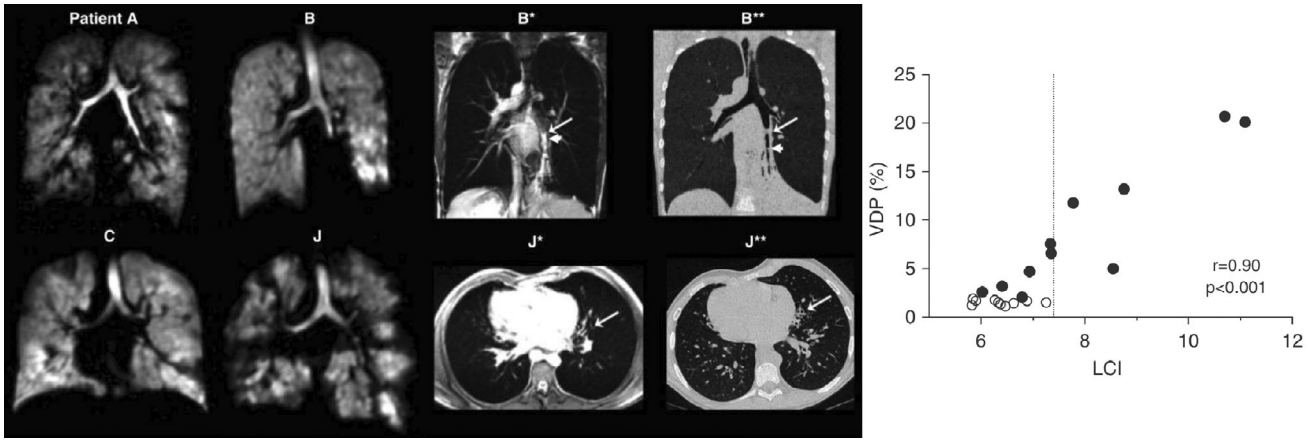


**FIGURE 12: $^{3}$He images of lung ventilation heterogeneity (left) alongside 3D SPGR images of two patients (B* and J*) and computed tomography images (B** and J**) in school-aged children with primary ciliary dyskinesia (PCD). Reprinted with permission of the American Thoracic Society.[151] Copyright © 2024 American Thoracic Society. All rights reserved. Annals of the American Thoracic Society is an official journal of the American Thoracic Society. Right: correlation of ventilation defect percentage (VDP) with the lung clearance index (LCI) metric derived from the multi-breath washout pulmonary function test. SPGR = spoiled gradient recalled echo.**

rapidly evolving to evaluate beyond morphology. Through ongoing collaboration between lung imaging centers and scanner vendors, substantial progress toward the integration of more specialized techniques into commercially available products is being made. This progress will lower the hurdle of accessibility to specialized sequences and techniques.

### *Accessibility of (Hyperpolarized Gas) Lung MRI*

Access to MRI scanners generally remains challenging, especially in developing countries, and as discussed in the following section, low-field and portable, low-cost MRI scanners have been developed to address this.[156,157] Nevertheless, access to hyperpolarized $^{129}$Xe polarizers and multi-nuclear hardware and software for MRI scanners is likely to remain restricted to specialized centers due to the significant start-up costs (up to $500 k for a polarizer, and potentially a similar cost to upgrade a $^{1}$H-only scanner to multi-nuclear capable). A reimbursement model at specialized regional/national referral centers may be achievable in certain developed countries. However, the extra running/prescription costs of $^{129}$Xe MRI also require consideration; the cost of enriched $^{129}$Xe is $150 ~ 300 per litre (with up to ~500 mL being used for a single ventilation scan). This reduces to ~$30 per litre for natural abundance xenon, which is similar to the cost of routine spirometry and may provide a more scalable route to widespread clinical use.

### *Changing Clinical Guidelines*

There is still further work to do to influence national/international guidelines on the use of MRI in pediatric lung disease. MRI is widely accepted at all CF centers in Germany, and by patient organizations.[158] This is recognized in the recent Fleischner Society guideline paper.[9] One example of the kind of work the research community needs to do for infant/pediatric lung MRI to influence clinical guidelines/decision-making more broadly is the work of Adaikalam and colleagues, who showed that the clinical decision-making process for tracheostomy procedures in infants with BPD can be guided by predictions from lung MRI.[90] Similar future studies around, eg, MRI-based characterization of the lung disease phenotypes in patients that most strongly correlate with response to certain clinical therapeutics will help guide clinicians in weighing-up the cost of therapeutics against their potential benefit in individual patients. Alongside this, we believe that additional research validating functional techniques in the pediatric setting is warranted to allow a widespread clinical application; for hyperpolarized gas MRI and non-contrast functional imaging such as Matrix Pencil/Fourier Decomposition and PREFUL MRI.

## Future Avenues

In this review, we have summarized the state-of-the-art in lung MRI methods and technology, and the current key areas where lung MRI shows utility in a clinical setting and should find increased application henceforth. In this concluding paragraph, we outline possible research directions for the field that are likely to be a focus of research efforts in the coming years. First, the recent resurgence in low-field MRI has potentially dramatic consequences for the lung MRI field, given the SNR improvement for $^{1}$H imaging of the lung parenchyma.[159] The reduced footprint is also attractive in terms of improved sustainability and increased accessibility, which may allow scanners to be placed closer to pediatric/neonatal wards. The advent of niche, cheap and portable low-field systems are promising for point-of-care brain imaging[160] but the attainable image quality in the lung is yet to be evaluated. Second, as MRI acquisition methods for the lung have matured, the focus of present research is showing a trend toward developing more robust and informative analyses, and the use of

artificial intelligence (AI) in lung image reconstruction,[161,162] segmentation,[163,164] functional mapping and registration.[165] To date the applications of AI in lung MRI have been limited to studies in adults, and this largely reflects the weighting of the training of these models toward images acquired in adults, and the larger "market" in terms of numbers of patients living with lung disease. In a recent review of the status of AI in chest CT and x-ray, although >20 AI products available for clinical use were reviewed, very few of these showed any application for pediatric imaging,[166] and we may expect a similar situation with MRI AI products. The ethical challenges governing the use of lung images from children to train AI models and how this differs from the situation in adults is beyond the scope of the current article,[167] but in the near future we would expect tailored AI for accelerated imaging and reconstruction of motion-artifact free images when AI models are trained with high SNR gated images in children. Furthermore, AI-driven protocolling should allow for rapid turnaround of pediatric scans, crucial for pre-school children in particular who may have limited compliance in the scanner. Finally, beyond lung imaging, MRI of the major airways has been relatively under-explored outside of the neonatal population,[90] but has the potential to inform treatment decisions—eg, reducing the number of invasive bronchoscopic procedures—in pediatric airway disorders such as obstructive sleep apnea, and can be acquired relatively easily in the same session as lung images.

## References


1. Wielputz MO, Puderbach M, Kopp-Schneider A, et al. Magnetic resonance imaging detects changes in structure and perfusion, and response to therapy in early cystic fibrosis lung disease. Am J Respir Crit Care Med 2014;189(8):956-965. https://doi.org/10.1164/rccm.201309-1659OC.
2. Roach DJ, Crémillieux Y, Fleck RJ, et al. Ultrashort echo-time magnetic resonance imaging is a sensitive method for the evaluation of early cystic fibrosis lung disease. Ann Am Thorac Soc 2016;13(11):1923-1931. https://doi.org/10.1513/AnnalsATS.201603-203OC.
3. Ohno Y, Takenaka D, Yoshikawa T, et al. Efficacy of ultrashort echo time pulmonary MRI for lung nodule detection and lung-RADS classification. Radiology 2022;302(3):697-706. https://doi.org/10.1148/radiol.211254.
4. Stewart NJ, Smith LJ, Chan HF, et al. Lung MRI with hyperpolarised gases: Current & future clinical perspectives. BJR 2022;95(1132):20210207. https://doi.org/10.1259/bjr.20210207.
5. Food and Drug Administration – Dose Prescription Information. XENOVIEW (xenon Xe 129 hyperpolarized), for oral inhalation. 2022. Reference ID: 5100335. Available from: https://www.accessdata.fda.gov/drugsatfda_docs/label/2022/214375s000lbl.pdf.
6. DiMango E, Spielman DB, Overdevest J, et al. Effect of highly effective modulator therapy on quality of life in adults with cystic fibrosis. Int Forum Allergy Rhinol 2021;11(1):75-78.
7. Abbas F, Georas S, Cai X, Khurana S. Asthma biologics: Real-world effectiveness, impact of switching biologics, and predictors of response. Ann Allergy Asthma Immunol 2021;127(6):655-660.e1. https://doi.org/10.1016/j.anai.2021.08.416.
8. Holland SK, Altaye M, Robertson S, Byars AW, Plante E, Szaflarski JP. Data on the safety of repeated MRI in healthy children. NeuroImage: Clin 2014;4:526-530. https://doi.org/10.1016/j.nicl.2014.01.013.
9. Hatabu H, Ohno Y, Gefter WB, et al. Expanding applications of pulmonary MRI in the clinical evaluation of lung disorders: Fleischner society position paper. Radiology 2020;297:201138. https://doi.org/10.1148/radiol.2020201138.
10. Duijts L, van Meel ER, Moschino L, et al. European Respiratory Society guideline on long-term management of children with bronchopulmonary dysplasia. Eur Respir J 2020;55(1):1900788. https://doi.org/10.1183/13993003.00788-2019.
11. Hatabu H, Alsop DC, Listerud J, Bonnet M, Gefter WB. T2* and proton density measurement of normal human lung parenchyma using submillisecond echo time gradient echo magnetic resonance imaging. Eur J Radiol 1999;29(3):245-252. https://doi.org/10.1016/S0720-048X(98)00169-7.
12. Yu J, Xue Y, Song HK. Comparison of lung T2* during free-breathing at 1.5 T and 3.0 T with ultrashort echo time imaging. Magn Reson Med 2011;66(1):248-254. https://doi.org/10.1002/mrm.22829.
13. Li B, Lee NG, Cui SX, Nayak KS. Lung parenchyma transverse relaxation rates at 0.55 T. Magn Reson Med 2023;89(4):1522-1530. https://doi.org/10.1002/mrm.29541.
14. Higano NS, Hahn AD, Tkach JA, et al. Retrospective respiratory self-gating and removal of bulk motion in pulmonary UTE MRI of neonates and adults. Magn Reson Med 2017;77(3):1284-1295. https://doi.org/10.1002/mrm.26212.
15. Fleming S, Thompson M, Stevens R, et al. Normal ranges of heart rate and respiratory rate in children from birth to 18 years of age: A systematic review of observational studies. Lancet 2011;377(9770):1011-1018. https://doi.org/10.1016/S0140-6736(10)62226-X.
16. Serai SD, Rapp JB, States LJ, Andronikou S, Ciet P, Lee EY. Pediatric lung MRI: Currently available and emerging techniques. Am J Roentgenol 2021;216(3):781-790. https://doi.org/10.2214/AJR.20.23104.
17. Zanette B, Greer MLC, Moraes TJ, Ratjen F, Santyr G. The argument for utilising magnetic resonance imaging as a tool for monitoring lung structure and function in pediatric patients. Expert Rev Respir Med 2023;17(7):527-538. https://doi.org/10.1080/17476348.2023.2241355.
18. Sodhi KS, Khandelwal N, Saxena AK, et al. Rapid lung MRI in children with pulmonary infections: Time to change our diagnostic algorithms. J Magn Reson Imaging 2016;43(5):1196-1206. https://doi.org/10.1002/jmri.25082.
19. Plathow C, Schoebinger M, Fink C, et al. Evaluation of lung volumetry using dynamic three-dimensional magnetic resonance imaging. Invest Radiol 2005;40(3):173-179.
20. Walkup LL, Tkach JA, Higano NS, et al. Quantitative magnetic resonance imaging of bronchopulmonary dysplasia in the neonatal intensive care unit environment. Am J Respir Crit Care Med 2015;192(10):1215-1222. https://doi.org/10.1164/rccm.201503-0552OC.
21. Ciet P, Wielopolski P, Manniesing R, et al. Spirometer-controlled cine magnetic resonance imaging used to diagnose tracheobronchomalacia in paediatric patients. Eur Respir J 2014;43(1):115-124. https://doi.org/10.1183/09031936.00104512.
22. Failo R, Wielopolski PA, Tiddens HAWM, Hop WCJ, Mucelli RP, Lequin MH. Lung morphology assessment using MRI: A robust ultrashort TR/TE 2D steady state free precession sequence used in cystic fibrosis patients. Magn Reson Med 2009;61(2):299-306. https://doi.org/10.1002/mrm.21841.
23. Bieri O. Ultra-fast steady state free precession and its application to in vivo 1H morphological and functional lung imaging at 1.5 tesla. Magn Reson Med 2013;70(3):657-663. https://doi.org/10.1002/mrm.24858.
24. Adams EW, Counsell SJ, Hajnal JV, Allsop JM, Herlihy A, Edwards AD. Investigation of lung disease in preterm infants using magnetic resonance imaging. Biol Neonate 2000;77(Suppl. 1):17-20. https://doi.org/10.1159/000047053.
25. Adams EW, Counsell SJ, Hajnal JV, et al. Magnetic resonance imaging of lung water content and distribution in term and preterm infants.

Am J Respir Crit Care Med 2002;166(3):397-402. https://doi.org/10.1164/rccm.2104116.

26. Hatabu H, Gaa J, Tadamura E, et al. MR imaging of pulmonary parenchyma with a half-Fourier single-shot turbo spin-echo (HASTE) sequence. Eur J Radiol 1999;29(2):152-159. https://doi.org/10.1016/S0720-048X(98)00167-3.

27. Puderbach M, Eichinger M, Haeselbarth J, et al. Assessment of morphological MRI for pulmonary changes in cystic fibrosis (CF) patients: Comparison to thin-section CT and chest X-ray. Invest Radiol 2007;42(10):715-724. https://doi.org/10.1097/RLI.0b013e318074fd81.

28. Fink C, Puderbach M, Biederer J, et al. Lung MRI at 1.5 and 3 tesla: Observer preference study and lesion contrast using five different pulse sequences. Invest Radiol 2007;42(6):377-383. https://doi.org/10.1097/01.rli.0000261926.86278.96.

29. Ciet P, Serra G, Bertolo S, et al. Assessment of CF lung disease using motion corrected PROPELLER MRI: A comparison with CT. Eur Radiol 2016;26(3):780-787. https://doi.org/10.1007/s00330-015-3850-9.

30. Sundgren PC, Leander P. Is administration of gadolinium-based contrast media to pregnant women and small children justified? J Magn Reson Imaging 2011;34(4):750-757. https://doi.org/10.1002/jmri.22413.

31. Saranathan M, Rettmann DW, Hargreaves BA, Clarke SE, Vasanawala SS. DIfferential subsampling with cartesian ordering (DISCO): A high spatio-temporal resolution dixon imaging sequence for multiphasic contrast enhanced abdominal imaging. J Magn Reson Imaging 2012;35(6):1484-1492. https://doi.org/10.1002/jmri.23602.

32. Feng L, Grimm R, Block KT, et al. Golden-angle radial sparse parallel MRI: Combination of compressed sensing, parallel imaging, and golden-angle radial sampling for fast and flexible dynamic volumetric MRI. Magn Reson Med 2014;72(3):707-717. https://doi.org/10.1002/mrm.24980.

33. Eichinger M, Optazaite DE, Kopp-Schneider A, et al. Morphologic and functional scoring of cystic fibrosis lung disease using MRI. Eur J Radiol 2012;81(6):1321-1329. https://doi.org/10.1016/j.ejrad.2011.02.045.

34. Kellenberger CJ, Amaxopoulou C, Moehrlen U, Bode PK, Jung A, Geiger J. Structural and perfusion magnetic resonance imaging of congenital lung malformations. Pediatr Radiol 2020;50(8):1083-1094. https://doi.org/10.1007/s00247-020-04658-5.

35. Ouyang M, Bao L. Gadolinium contrast agent deposition in children. J Magn Reson Imaging 2024. https://doi.org/10.1002/jmri.29389.

36. Johnson KM, Fain SB, Schiebler ML, Nagle S. Optimized 3D ultrashort echo time pulmonary MRI. Magn Reson Med 2013;70(5):1241-1250. https://doi.org/10.1002/mrm.24570.

37. Hahn AD, Higano NS, Walkup LL, et al. Pulmonary MRI of neonates in the intensive care unit using 3D ultrashort echo time and a small footprint MRI system. J Magn Reson Imaging 2017;45(2):463-471. https://doi.org/10.1002/jmri.25394.

38. Higano NS, Fleck RJ, Spielberg DR, et al. Quantification of neonatal lung parenchymal density via ultrashort echo time MRI with comparison to CT. J Magn Reson Imaging 2017;46(4):992-1000. https://doi.org/10.1002/jmri.25643.

39. Heidenreich JF, Veldhoen S, Metz C, et al. Functional MRI of the lungs using single breath-hold and self-navigated ultrashort echo time sequences. Radiol: Cardiothorac Imaging 2020;2(3):e190162. https://doi.org/10.1148/ryct.2020190162.

40. Heidenreich JF, Weng AM, Metz C, et al. Three-dimensional ultrashort echo time MRI for functional lung imaging in cystic fibrosis. Radiology 2020;296(1):191-199. https://doi.org/10.1148/radiol.2020192251.

41. Pipe JG, Zwart NR, Aboussouan EA, Robison RK, Devaraj A, Johnson KO. A new design and rationale for 3D orthogonally oversampled k-space trajectories. Magn Reson Med 2011;66(5):1303-1311. https://doi.org/10.1002/mrm.22918.

42. Willmering MM, Robison RK, Wang H, Pipe JG, Woods JC. Implementation of the FLORET UTE sequence for lung imaging. Magn Reson Med 2019;82:1091-1100. https://doi.org/10.1002/mrm.27800.

43. Hahn AD, Higano NS, Willmering MM, Stewart NJ, Woods JC, Fain SB. Improving efficiency of ultra-short echo time MRI in neonatal lungs with a FLORET spiral trajectory. *International Society for Magnetic Resonance in Medicine Annual Meeting, London*. Concord, CA: International Society for Magnetic Resonance in Medicine; 2022. p 664.

44. Gibiino F, Sacolick L, Menini A, Landini L, Wiesinger F. Free-breathing, zero-TE MR lung imaging. Magn Reson Mater Phy 2015;28(3):207-215. https://doi.org/10.1007/s10334-014-0459-y.

45. Boucneau T, Fernandez B, Larson P, Darrasse L, Maître X. 3D magnetic resonance spirometry. Sci Rep 2020;10(1):9649. https://doi.org/10.1038/s41598-020-66202-7.

46. Papp D, Elders B, Wielopolski PA, et al. Lung parenchyma and structure visualisation in paediatric chest MRI: A comparison of different short and ultra-short echo time protocols. Clin Radiol 2023;78(4):e319-e327. https://doi.org/10.1016/j.crad.2022.12.020.

47. Mendes Pereira L, Wech T, Weng AM, et al. UTE-SENCEFUL: First results for 3D high-resolution lung ventilation imaging. Magn Reson Med 2019;81(4):2464-2473. https://doi.org/10.1002/mrm.27576.

48. Feng L, Axel L, Chandarana H, Block KT, Sodickson DK, Otazo R. XD-GRASP: Golden-angle radial MRI with reconstruction of extra motion-state dimensions using compressed sensing. Magn Reson Med 2016;75(2):775-788. https://doi.org/10.1002/mrm.25665.

49. Zhu X, Chan M, Lustig M, Johnson KM, Larson PEZ. Iterative motion-compensation reconstruction ultra-short TE (iMoCo UTE) for high-resolution free-breathing pulmonary MRI. Magn Reson Med 2019;83:1208-1221. https://doi.org/10.1002/mrm.27998.

50. Zou Q, Torres LA, Fain SB, Higano NS, Bates AJ, Jacob M. Dynamic imaging using motion-compensated smoothness regularization on manifolds (MoCo-SToRM). Phys Med Biol 2022;67(14):144001. https://doi.org/10.1088/1361-6560/ac79fc.

51. Tan F, Zhu X, Chan M, et al. Motion-compensated low-rank reconstruction for simultaneous structural and functional UTE lung MRI. Magn Reson Med 2023;90(3):1101-1113. https://doi.org/10.1002/mrm.29703.

52. Frahm J, Voit D, Uecker M. Real-time magnetic resonance imaging: Radial gradient-echo sequences with nonlinear inverse reconstruction. Invest Radiol 2019;54(12):757-766. https://doi.org/10.1097/RLI.0000000000000584.

53. Hirsch FW, Sorge I, Voit D, et al. Chest examinations in children with real-time magnetic resonance imaging: First clinical experience. Pediatr Radiol 2023;53(1):12-20. https://doi.org/10.1007/s00247-022-05421-8.

54. Niedbalski PJ, Hall CS, Castro M, et al. Protocols for multi-site trials using hyperpolarized 129Xe MRI for imaging of ventilation, alveolar-airspace size, and gas exchange: A position paper from the 129Xe MRI clinical trials consortium. Magn Reson Med 2021;86(6):2966-2986. https://doi.org/10.1002/mrm.28985.

55. Tzeng YS, Lutchen K, Albert M. The difference in ventilation heterogeneity between asthmatic and healthy subjects quantified using hyperpolarized 3He MRI. J Appl Physiol 2009;106(3):813-822. https://doi.org/10.1152/japplphysiol.01133.2007.

56. He M, Kaushik SS, Robertson SH, et al. Extending semiautomatic ventilation defect analysis for hyperpolarized 129Xe ventilation MRI. Acad Radiol 2014;21(12):1530-1541. https://doi.org/10.1016/J.ACRA.2014.07.017.

57. Horn FC, Deppe MH, Marshall H, Parra-Robles J, Wild JM. Quantification of regional fractional ventilation in human subjects by measurement of hyperpolarized $^{3}$He washout with 2D and 3D MRI. J Appl Physiol 2014;116(2):129-139. https://doi.org/10.1152/japplphysiol.00378.2013.

58. Couch MJ, Morgado F, Kanhere N, et al. Assessing the feasibility of hyperpolarized 129Xe multiple-breath washout MRI in pediatric cystic fibrosis. Magn Reson Med 2019;84:304-311. https://doi.org/10.1002/mrm.28099.

59. Kaushik SS, Cleveland ZI, Cofer GP, et al. Diffusion-weighted hyperpolarized 129Xe MRI in healthy volunteers and subjects with

chronic obstructive pulmonary disease. Magn Reson Med 2011;65(4):1154-1165. https://doi.org/10.1002/mrm.22697.

60. Yablonskiy DA, Sukstanskii AL, Leawoods JC, et al. Quantitative in vivo assessment of lung microstructure at the alveolar level with hyperpolarized 3He diffusion MRI. Proc Natl Acad Sci U S A 2002;99(5):3111-3116. https://doi.org/10.1073/pnas.052594699.

61. Parra-Robles J, Marshall H, Wild JM. Characterization of $^{3}$He diffusion in lungs using a stretched exponential model. *International Society for Magnetic Resonance in Medicine Annual Meeting, Salt Lake City*. Concord, CA: International Society for Magnetic Resonance in Medicine; 2013. p 820.

62. Chan HF, Collier GJ, Weatherley ND, Wild JM. Comparison of in vivo lung morphometry models from 3D multiple b-value 3He and 129Xe diffusion-weighted MRI. Magn Reson Med 2019;81(5):2959-2971. https://doi.org/10.1002/mrm.27608.

63. Kaushik SS, Freeman MS, Yoon SW, et al. Measuring diffusion limitation with a perfusion-limited gas—Hyperpolarized 129Xe gas-transfer spectroscopy in patients with idiopathic pulmonary fibrosis. J Appl Physiol 2014;117(6):577-585. https://doi.org/10.1152/japplphysiol.00326.2014.

64. Zanette B, Santyr G. Accelerated interleaved spiral-IDEAL imaging of hyperpolarized 129Xe for parametric gas exchange mapping in humans. Magn Reson Med 2019;82(3):1113-1119. https://doi.org/10.1002/mrm.27765.

65. Stewart NJ, Leung G, Norquay G, et al. Experimental validation of the hyperpolarized 129Xe chemical shift saturation recovery technique in healthy volunteers and subjects with interstitial lung disease. Magn Reson Med 2015;74(1):196-207. https://doi.org/10.1002/mrm.25400.

66. Kaushik SS, Robertson SH, Freeman MS, et al. Single-breath clinical imaging of hyperpolarized $^{129}$Xe in the airspaces, barrier, and red blood cells using an interleaved 3D radial 1-point Dixon acquisition. Magn Reson Med 2016;75(4):1434-1443. https://doi.org/10.1002/mrm.25675.

67. Collier GJ, Eaden JA, Hughes PJC, et al. Dissolved $^{129}$Xe lung MRI with four-echo 3D radial spectroscopic imaging: Quantification of regional gas transfer in idiopathic pulmonary fibrosis. Magn Reson Med 2021;85(5):2622-2633. https://doi.org/10.1002/mrm.28609.

68. Qing K, Ruppert K, Jiang Y, et al. Regional mapping of gas uptake by blood and tissue in the human lung using hyperpolarized xenon-129 MRI. J Magn Reson Imaging 2014;39(2):346-359. https://doi.org/10.1002/jmri.24181.

69. Plummer JW, Willmering MM, Cleveland ZI, Towe C, Woods JC, Walkup LL. Childhood to adulthood: Accounting for age dependence in healthy-reference distributions in $^{129}$Xe gas-exchange MRI. Magn Reson Med 2023;89(3):1117-1133. https://doi.org/10.1002/mrm.29501.

70. Willmering MM, Walkup LL, Niedbalski PJ, et al. Pediatric $^{129}$Xe gas-transfer MRI—Feasibility and applicability. J Magn Reson Imaging 2022;56(4):1207-1219. https://doi.org/10.1002/jmri.28136.

71. Quanjer PH, Stanojevic S, Cole TJ, et al. Multi-ethnic reference values for spirometry for the 3–95-yr age range: The global lung function 2012 equations. Eur Respir J 2012;40(6):1324-1343. https://doi.org/10.1183/09031936.00080312.

72. Shukla Y, Wheatley A, Kirby M, et al. Hyperpolarized 129Xe magnetic resonance imaging: Tolerability in healthy volunteers and subjects with pulmonary disease. Acad Radiol 2012;19(8):941-951. https://doi.org/10.1016/J.ACRA.2012.03.018.

73. Walkup LL, Thomen RP, Akinyi TG, et al. Feasibility, tolerability and safety of pediatric hyperpolarized 129Xe magnetic resonance imaging in healthy volunteers and children with cystic fibrosis. Pediatr Radiol 2016;46(12):1651-1662. https://doi.org/10.1007/s00247-016-3672-1.

74. Stewart NJ, Higano NS, Mukthapuram S, et al. Initial feasibility and challenges of hyperpolarized 129Xe MRI in neonates with bronchopulmonary dysplasia. Magn Reson Med 2023;90:2420-2431. https://doi.org/10.1002/mrm.29808.

75. Couch MJ, Ball IK, Li T, Fox MS, Biman B, Albert MS. $^{19}$F MRI of the lungs using inert fluorinated gases: Challenges and new developments. J Magn Reson Imaging 2019;49(2):343-354. https://doi.org/10.1002/jmri.26292.

76. McCallister A, Chung SH, Antonacci M, et al. Comparison of single breath hyperpolarized $^{129}$Xe MRI with dynamic $^{19}$F MRI in cystic fibrosis lung disease. Magn Reson Med 2020;85:1028-1038. https://doi.org/10.1002/mrm.28457.

77. Zanette B, Alam F, Neal MA, Thelwall PE, Ratjen F, Santyr GE. Preliminary investigation of feasibility, tolerability, and image quality of perfluoropropane ventilation MRI in pediatric participants. *International Society for Magnetic Resonance in Medicine Annual Meeting, Singapore*. Concord, CA: International Society for Magnetic Resonance in Medicine; 2024. p 64.

78. Bauman G, Puderbach M, Deimling M, et al. Non-contrast-enhanced perfusion and ventilation assessment of the human lung by means of Fourier decomposition in proton MRI. Magn Reson Med 2009;62(3):656-664. https://doi.org/10.1002/mrm.22031.

79. Fischer A, Weick S, Ritter CO, et al. SElf-gated Non-Contrast-Enhanced FUnctional Lung imaging (SENCEFUL) using a quasi-random fast low-angle shot (FLASH) sequence and proton MRI. NMR Biomed 2014;27(8):907-917. https://doi.org/10.1002/nbm.3134.

80. Bauman G, Bieri O. Matrix pencil decomposition of time-resolved proton MRI for robust and improved assessment of pulmonary ventilation and perfusion. Magn Reson Med 2017;77(1):336-342. https://doi.org/10.1002/mrm.26096.

81. Voskrebenzev A, Gutberlet M, Klimeš F, et al. Feasibility of quantitative regional ventilation and perfusion mapping with phase-resolved functional lung (PREFUL) MRI in healthy volunteers and COPD, CTEPH, and CF patients. Magn Reson Med 2018;79(4):2306-2314. https://doi.org/10.1002/mrm.26893.

82. Zanette B, Schrauben EM, Munidasa S, et al. Clinical feasibility of structural and functional MRI in free-breathing neonates and infants. J Magn Reson Imaging 2022;55(6):1696-1707. https://doi.org/10.1002/jmri.28165.

83. Klimeš F, Voskrebenzev A, Gutberlet M, et al. 3D phase-resolved functional lung ventilation MR imaging in healthy volunteers and patients with chronic pulmonary disease. Magn Reson Med 2021;85(2):912-925. https://doi.org/10.1002/mrm.28482.

84. Edelman RR, Hatabu H, Tadamura E, Li W, Prasad PV. Noninvasive assessment of regional ventilation in the human lung using oxygen-enhanced magnetic resonance imaging. Nat Med 1996;2(11):1236-1239. https://doi.org/10.1038/nm1196-1236.

85. Jakob PM, Wang T, Schultz G, Hebestreit H, Hebestreit A, Hahn D. Assessment of human pulmonary function using oxygen-enhanced T1 imaging in patients with cystic fibrosis. Magn Reson Med 2004;51(5):1009-1016. https://doi.org/10.1002/mrm.20051.

86. Wielpütz MO, von Stackelberg O, Stahl M, et al. Multicentre standardisation of chest MRI as radiation-free outcome measure of lung disease in young children with cystic fibrosis. J Cyst Fibros 2018;17(4):518-527. https://doi.org/10.1016/j.jcf.2018.05.003.

87. Sodhi KS, Ciet P, Vasanawala S, Biederer J. Practical protocol for lung magnetic resonance imaging and common clinical indications. Pediatr Radiol 2022;52(2):295-311. https://doi.org/10.1007/s00247-021-05090-z.

88. Ochiai M, Hikino S, Yabuuchi H, et al. A new scoring system for computed tomography of the chest for assessing the clinical status of bronchopulmonary dysplasia. J Pediatr 2008;152(1):90-95.e3. https://doi.org/10.1016/j.jpeds.2007.05.043.

89. Higano NS, Spielberg DR, Fleck RJ, et al. Neonatal pulmonary MRI of bronchopulmonary dysplasia predicts short-term clinical outcomes. Am J Respir Crit Care Med 2018;198:1302-1311. https://doi.org/10.1164/rccm.201711-2287OC.

90. Adaikalam SA, Higano NS, Hysinger EB, et al. Tracheostomy prediction model in neonatal bronchopulmonary dysplasia via lung and airway MRI. Pediatr Pulmonol 2022;57(4):1042-1050. https://doi.org/10.1002/ppul.25826.

91. Förster K, Marchi H, Stöcklein S, et al. MRI based scoring of the diseased lung in the preterm infant with BPD. Am J Physiol Lung Cell

Mol Physiol 2022;324:L114-L122. https://doi.org/10.1152/ajplung.00430.2021.

92. Higano NS, Fleck RJ, Schapiro AH, et al. Objective lung-density quantification in neonatal bronchopulmonary dysplasia via ultrashort echo-time MRI, with comparison to clinical severity and reader scoring. *International Society for Magnetic Resonance in Medicine, Montreal*. Concord, CA: International Society for Magnetic Resonance in Medicine; 2019. p 1111.

93. Hahn AD, Malkus A, Kammerman J, et al. Characterization of and tissue density in the human lung: Application to neonatal imaging in the intensive care unit. Magn Reson Med 2020;84(2):920-927. https://doi.org/10.1002/mrm.28137.

94. Hahn AD, Malkus A, Kammerman J, et al. Effects of neonatal lung abnormalities on parenchymal R2* estimates. J Magn Reson Imaging 2021;53(6):1853-1861. https://doi.org/10.1002/jmri.27487.

95. Schopper MA, Walkup LL, Tkach JA, et al. Evaluation of neonatal lung volume growth by pulmonary magnetic resonance imaging in patients with congenital diaphragmatic hernia. J Pediatr 2017;188:96-102.e1. https://doi.org/10.1016/j.jpeds.2017.06.002.

96. Adaikalam SA, Higano NS, Tkach JA, et al. Neonatal lung growth in congenital diaphragmatic hernia: Evaluation of lung density and mass by pulmonary MRI. Pediatr Res 2019;86:635-640. https://doi.org/10.1038/s41390-019-0480-y.

97. Mairhörmann B, Castelblanco A, Häfner F, et al. Automated MRI lung segmentation and 3D morphologic features for quantification of neonatal lung disease. Radiol: Artif Intell 2023;5(6):e220239. https://doi.org/10.1148/ryai.220239.

98. Gouwens KR, Higano NS, Marks KT, et al. MRI evaluation of regional lung tidal volumes in severe neonatal bronchopulmonary dysplasia. Am J Respir Crit Care Med 2020;202(7):1024-1031. https://doi.org/10.1164/rccm.202001-0213oc.

99. Yoder LM, Higano NS, Schapiro AH, et al. Elevated lung volumes in neonates with bronchopulmonary dysplasia measured via MRI. Pediatr Pulmonol 2019;54(8):1311-1318. https://doi.org/10.1002/ppul.24378.

100. Katz SL, Parraga G, Luu TM, et al. Pulmonary magnetic resonance imaging of ex-preterm children with and without bronchopulmonary dysplasia. Ann ATS 2022;19(7):1149-1157. https://doi.org/10.1513/AnnalsATS.202106-691OC.

101. Dyke JP, Voskrebenzev A, Blatt LK, et al. Assessment of lung ventilation and perfusion of premature infants with bronchopulmonary dysplasia at 1.5 tesla using phase-resolved functional lung (PREFUL) magnetic resonance imaging (MRI) in the NICU. Pediatr Radiol 2023;53:1076-1084. https://doi.org/10.21203/rs.3.rs-1765576/v1.

102. Altes TA, Meyer CH, Mata JF, et al. Hyperpolarized helium-3 magnetic resonance lung imaging of non-sedated infants and young children: A proof-of-concept study. Clin Imaging 2017;45:105-110. https://doi.org/10.1016/J.CLINIMAG.2017.04.004.

103. Higano NS, Thomen RP, Quirk JD, et al. Alveolar airspace size in healthy and diseased infant lungs measured via hyperpolarized $^{3}$He gas diffusion magnetic resonance imaging. Neo 2020;117(6):704-712. https://doi.org/10.1159/000511084.

104. Flors L, Mugler JP, Paget-Brown A, et al. Hyperpolarized Helium-3 diffusion-weighted magnetic resonance imaging detects abnormalities of lung structure in children with bronchopulmonary dysplasia. J Thorac Imaging 2017;32(5):323-332. https://doi.org/10.1097/RTI.0000000000000244.

105. Chan HF, Smith LJ, Biancardi AM, et al. Image phenotyping of preterm-born children using hyperpolarised $^{129}$Xe lung MRI and multiple-breath washout. Am J Respir Crit Care Med 2023;207(1):89-100. https://doi.org/10.1164/rccm.202203-0606OC.

106. Narayanan M, Beardsmore CS, Owers-Bradley J, et al. Catch-up alveolarization in ex-preterm children. Evidence from $^{3}$He magnetic resonance. Am J Respir Crit Care Med 2013;187(10):1104-1109. https://doi.org/10.1164/rccm.201210-1850OC.

107. Parra-Robles J, Wild JM. On the use of $^{3}$He diffusion magnetic resonance as evidence of neo-alveolarization during childhood and adolescence. Am J Respir Crit Care Med 2014;189(4):501-502. https://doi.org/10.1164/rccm.201309-1650LE.

108. Elders BBLJ, Tiddens HAWM, Pijnenburg MWH, Reiss IKM, Wielopolski PA, Ciet P. Lung structure and function on MRI in preterm born school children with and without BPD: A feasibility study. Pediatr Pulmonol 2022;57(12):2981-2991. https://doi.org/10.1002/ppul.26119.

109. Narayanan M, Owers-Bradley J, Beardsmore CS, et al. Alveolarization continues during childhood and adolescence: New evidence from helium-3 magnetic resonance. Am J Respir Crit Care Med 2012;185(2):186-191. https://doi.org/10.1164/rccm.201107-1348OC.

110. Bell SC, Mall MA, Gutierrez H, et al. The future of cystic fibrosis care: A global perspective. Lancet Respir Med 2020;8(1):65-124. https://doi.org/10.1016/S2213-2600(19)30337-6.

111. Grasemann H, Ratjen F. Early lung disease in cystic fibrosis. Lancet Respir Med 2013;1(2):148-157. https://doi.org/10.1016/S2213-2600(13)70026-2.

112. Stick S, Tiddens H, Aurora P, et al. Early intervention studies in infants and preschool children with cystic fibrosis: Are we ready? Eur Respir J 2013;42(2):527-538. https://doi.org/10.1183/09031936.00108212.

113. Sly PD, Wainwright CE. Diagnosis and early life risk factors for bronchiectasis in cystic fibrosis: A review. Expert Rev Respir Med 2016;10(9):1003-1010. https://doi.org/10.1080/17476348.2016.1204915.

114. Stahl M, Steinke E, Graeber SY, et al. Magnetic resonance imaging detects progression of lung disease and impact of newborn screening in preschool children with cystic fibrosis. Am J Respir Crit Care Med 2021;204(8):943-953. https://doi.org/10.1164/rccm.202102-0278OC.

115. Biederer J, Both M, Graessner J, et al. Lung morphology: Fast MR imaging assessment with a volumetric interpolated breath-hold technique: Initial experience with patients. Radiology 2003;226(1):242-249. https://doi.org/10.1148/radiol.2261011974.

116. Puderbach M, Eichinger M, Gahr J, et al. Proton MRI appearance of cystic fibrosis: Comparison to CT. Eur Radiol 2007;17(3):716-724. https://doi.org/10.1007/s00330-006-0373-4.

117. Mall MA, Stahl M, Graeber SY, Sommerburg O, Kauczor HU, Wielpütz MO. Early detection and sensitive monitoring of CF lung disease: Prospects of improved and safer imaging. Pediatric Pulmonology 2016;51(544):S49-S60.

118. Stahl M, WielpüTz MO, Graeber SY, et al. Comparison of lung clearance index and magnetic resonance imaging for assessment of lung disease in children with cystic fibrosis. Am J Respir Crit Care Med 2017;195(3):349-359. https://doi.org/10.1164/rccm.201604-0893OC.

119. Wielputz M, Kauczor H u. MRI of the lung – State of the art. Diagn Interv Radiol 2012;18:344-353. https://doi.org/10.4261/1305-3825.DIR.5365-11.0.

120. Hopkins SR, Wielpütz MO, Kauczor HU. Imaging lung perfusion. J Appl Physiol 2012;113(2):328-339. https://doi.org/10.1152/japplphysiol.00320.2012.

121. Graeber SY, Renz DM, Stahl M, et al. Effects of Elexacaftor/Tezacaftor/Ivacaftor therapy on lung clearance index and magnetic resonance imaging in patients with cystic fibrosis and one or two F508del alleles. Am J Respir Crit Care Med 2022;206(3):311-320. https://doi.org/10.1164/rccm.202201-0219OC.

122. Graeber SY, Boutin S, Wielpütz MO, et al. Effects of Lumacaftor–Ivacaftor on lung clearance index, magnetic resonance imaging, and airway microbiome in Phe508del homozygous patients with cystic fibrosis. Ann ATS 2021;18(6):971-980. https://doi.org/10.1513/AnnalsATS.202008-1054OC.

123. Nyilas S, Bauman G, Pusterla O, et al. Ventilation and perfusion assessed by functional MRI in children with CF: Reproducibility in comparison to lung function. J Cyst Fibros 2019;18(4):543-550. https://doi.org/10.1016/j.jcf.2018.10.003.

124. Willers CC, Frauchiger BS, Stranzinger E, et al. Feasibility of unsedated lung MRI in young children with cystic fibrosis. Eur Respir J 2022;60(5):2103112. https://doi.org/10.1183/13993003.03112-2021.

125. Bauman G, Puderbach M, Heimann T, et al. Validation of Fourier decomposition MRI with dynamiccontrast-enhanced MRI using visual and automated scoring of pulmonary perfusion in young cystic fibrosis patients. Eur J Radiol 2013;82(12):2371-2377. https://doi.org/10.1016/j.ejrad.2013.08.018.

126. Munidasa S, Couch MJ, Rayment JH, et al. Free-breathing MRI for monitoring ventilation changes following antibiotic treatment of pulmonary exacerbations in paediatric cystic fibrosis. Eur Respir J 2021;57(4):2003104. https://doi.org/10.1183/13993003.03104-2020.

127. Kieninger E, Willers C, Röthlisberger K, et al. Effect of salbutamol on lung ventilation in children with cystic fibrosis: Comprehensive assessment using spirometry, multiple-breath washout, and functional lung magnetic resonance imaging. Respiration 2021;101(3):281-290. https://doi.org/10.1159/000519751.

128. Streibel C, Willers CC, Pusterla O, et al. Effects of elexacaftor/tezacaftor/ivacaftor therapy in children with cystic fibrosis – A comprehensive assessment using lung clearance index, spirometry, and functional and structural lung MRI. J Cyst Fibros 2023;22(4):615-622. https://doi.org/10.1016/j.jcf.2022.12.012.

129. Koumellis P, van Beek EJR, Woodhouse N, et al. Quantitative analysis of regional airways obstruction using dynamic hyperpolarized3He MRI—Preliminary results in children with cystic fibrosis. J Magn Reson Imaging 2005;22(3):420-426. https://doi.org/10.1002/jmri.20402.

130. Smith L, Marshall H, Aldag I, et al. Longitudinal assessment of children with mild cystic fibrosis using hyperpolarized gas lung magnetic resonance imaging and lung clearance index. Am J Respir Crit Care Med 2018;197(3):397-400. https://doi.org/10.1164/rccm.201705-0894LE.

131. Kanhere N, Couch MJ, Kowalik K, et al. Correlation of lung clearance index with hyperpolarized $^{129}$Xe magnetic resonance imaging in pediatric subjects with cystic fibrosis. Am J Respir Crit Care Med 2017;196(8):1073-1075. https://doi.org/10.1164/rccm.201611-2228LE.

132. Thomen RP, Walkup LL, Roach DJ, Cleveland ZI, Clancy JP, Woods JC. Hyperpolarized $^{129}$Xe for investigation of mild cystic fibrosis lung disease in pediatric patients. J Cyst Fibros 2017;16(2):275-282. https://doi.org/10.1016/J.JCF.2016.07.008.

133. Marshall H, Horsley A, Taylor CJ, et al. Detection of early subclinical lung disease in children with cystic fibrosis by lung ventilation imaging with hyperpolarised gas MRI. Thorax 2017;72(8):760-762. https://doi.org/10.1136/thoraxjnl-2016-208948.

134. Smith LJ, Horsley A, Bray J, et al. The assessment of short- and long-term changes in lung function in cystic fibrosis using $^{129}$Xe MRI. Eur Respir J 2020;56(6):2000441. https://doi.org/10.1183/13993003.00441-2020.

135. Woodhouse N, Wild JM, van Beek EJR, Hoggard N, Barker N, Taylor CJ. Assessment of hyperpolarized 3He lung MRI for regional evaluation of interventional therapy: A pilot study in pediatric cystic fibrosis. J Magn Reson Imaging 2009;30(5):981-988. https://doi.org/10.1002/jmri.21949.

136. Bannier E, Cieslar K, Mosbah K, et al. Hyperpolarized $^{3}$He MR for sensitive imaging of ventilation function and treatment efficiency in young cystic fibrosis patients with normal lung function. Radiology 2010;255(1):225-232. https://doi.org/10.1148/radiol.09090039.

137. Smith LJ, Marshall H, Bray J, et al. The effect of acute maximal exercise on the regional distribution of ventilation using ventilation MRI in CF. J Cyst Fibros 2020;20:625-631. https://doi.org/10.1016/j.jcf.2020.08.009.

138. Altes TA, Johnson M, Fidler M, et al. Use of hyperpolarized helium-3 MRI to assess response to ivacaftor treatment in patients with cystic fibrosis. J Cyst Fibros 2017;16(2):267-274. https://doi.org/10.1016/j.jcf.2016.12.004.

139. Rayment JH, Couch MJ, McDonald N, et al. Hyperpolarised $^{129}$Xe magnetic resonance imaging to monitor treatment response in children with cystic fibrosis. Eur Respir J 2019;53(5):1802188. https://doi.org/10.1183/13993003.02188-2018.

140. Marshall H, Voskrebenzev A, Smith LJ, et al. $^{129}$Xe and free-breathing 1H ventilation MRI in patients with cystic fibrosis: A dual-center study. J Magn Reson Imaging 2023;57(6):1908-1921. https://doi.org/10.1002/jmri.28470.

141. Couch MJ, Munidasa S, Rayment JH, et al. Comparison of functional free-breathing pulmonary 1H and hyperpolarized $^{129}$Xe magnetic resonance imaging in pediatric cystic fibrosis. Acad Radiol 2020;28(8):e209-e218. https://doi.org/10.1016/j.acra.2020.05.008.

142. Munidasa S, Zanette B, Couch M, et al. Inter- and intravisit repeatability of free-breathing MRI in pediatric cystic fibrosis lung disease. Magn Reson Med 2023;89(5):2048-2061. https://doi.org/10.1002/mrm.29566.

143. Couch MJ, Thomen R, Kanhere N, et al. A two-center analysis of hyperpolarized 129 Xe lung MRI in stable pediatric cystic fibrosis: Potential as a biomarker for multi-site trials. J Cyst Fibros 2019;18:728-733. https://doi.org/10.1016/j.jcf.2019.03.005.

144. Tsuchiya N, Schiebler ML, Evans MD, et al. Safety of repeated hyperpolarized helium 3 magnetic resonance imaging in pediatric asthma patients. Pediatr Radiol 2020;50:646-655. https://doi.org/10.1007/s00247-019-04604-0.

145. Cadman RV, Lemanske RF, Evans MD, et al. Pulmonary 3He magnetic resonance imaging of childhood asthma. J Allergy Clin Immunol 2013;131(2):369-376.e5. https://doi.org/10.1016/j.jaci.2012.10.032.

146. Altes TA, Mugler JP, Ruppert K, et al. Clinical correlates of lung ventilation defects in asthmatic children. J Allergy Clin Immunol 2016;137(3):789-796.e7. https://doi.org/10.1016/j.jaci.2015.08.045.

147. Lin NY, Roach DJ, Willmering MM, et al. $^{129}$Xe MRI as a measure of clinical disease severity for pediatric asthma. J Allergy Clin Immunol 2020;147:2146-2153.e1. https://doi.org/10.1016/j.jaci.2020.11.010.

148. Safavi S, Munidasa S, Zanette B, et al. Evaluating post-bronchodilator response in well-controlled paediatric severe asthma using hyperpolarised 129Xe-MRI: A pilot study. Respir Med 2021;180:106368. https://doi.org/10.1016/j.rmed.2021.106368.

149. Maglione M, Montella S, Mollica C, et al. Lung structure and function similarities between primary ciliary dyskinesia and mild cystic fibrosis: A pilot study. Ital J Pediatr 2017;43(1):34. https://doi.org/10.1186/s13052-017-0351-2.

150. Nyilas S, Bauman G, Pusterla O, et al. Structural and functional lung impairment in primary ciliary dyskinesia. Assessment with magnetic resonance imaging and multiple breath washout in comparison to spirometry. Ann ATS 2018;15(12):1434-1442. https://doi.org/10.1513/AnnalsATS.201712-967OC.

151. Smith LJ, West N, Hughes D, et al. Imaging lung function abnormalities in primary ciliary dyskinesia using hyperpolarized gas ventilation MRI. Ann Am Thorac Soc 2018;15(12):1487-1490. https://doi.org/10.1513/AnnalsATS.201711-890RL.

152. Wee W, Zanette B, Munidasa S, et al. Multisite hyperpolarized $^{129}$Xe MRI study of pediatric primary ciliary dyskinesia. Eur Respir J 2023;62-(suppl 67):PA3995. https://doi.org/10.1183/13993003.congress-2023.PA3995.

153. Sodhi KS, Sharma M, Lee EY, et al. Diagnostic utility of 3T lung MRI in children with interstitial lung disease: A prospective pilot study. Acad Radiol 2018;25(3):380-386. https://doi.org/10.1016/j.acra.2017.09.013.

154. Walkup LL, Myers KC, El-Bietar J, Gloude NJ, Towe C, Woods JC. Regional lung ventilation deficits in pediatric hematopoietic stem cell transplant patients revealed via hyperpolarized Xenon-129 magnetic resonance imaging. Biol Blood Marrow Transplant 2018;24(3):S66. https://doi.org/10.1016/j.bbmt.2017.12.636.

155. Copeland A, Silver E, Korja R, et al. Infant and child MRI: A review of scanning procedures. Front Neurosci 2021;15:15. https://doi.org/10.3389/fnins.2021.666020.

156. Wald LL, McDaniel PC, Witzel T, Stockmann JP, Cooley CZ. Low-cost and portable MRI. J Magn Reson Imaging 2020;52(3):686-696. https://doi.org/10.1002/jmri.26942.

157. Arnold TC, Freeman CW, Litt B, Stein JM. Low-field MRI: Clinical promise and challenges. J Magn Reson Imaging 2023;57(1):25-44. https://doi.org/10.1002/jmri.28408.

158. Leutz-Schmidt P, Eichinger M, Stahl M, et al. Ten years of chest MRI for patients with cystic fibrosis. Radiologe 2019;59(1):10-20. https://doi.org/10.1007/s00117-019-0553-2.

159. Campbell-Washburn AE, Ramasawmy R, Restivo MC, et al. Opportunities in interventional and diagnostic imaging by using high-performance low-field-strength MRI. Radiology 2019;293(2):384-393. https://doi.org/10.1148/radiol.2019190452.

160. Sheth KN, Mazurek MH, Yuen MM, et al. Assessment of brain injury using portable, low-field magnetic resonance imaging at the bedside of critically ill patients. JAMA Neurol 2021;78(1):41-47. https://doi.org/10.1001/jamaneurol.2020.3263.

161. Bae K, Lee J, Jung Y, de Arcos J, Jeon KN. Deep learning reconstruction for zero echo time lung magnetic resonance imaging: Impact on image quality and lesion detection. Clin Radiol 2024;79:e1296-e1303. https://doi.org/10.1016/j.crad.2024.07.011.

162. Stewart NJ, de Arcos J, Biancardi AM, et al. Improving Xenon-129 lung ventilation image SNR with deep-learning based image reconstruction. Magn Reson Med 2024;92:2546-2559. https://doi.org/10.1002/mrm.30250.

163. Willers C, Bauman G, Andermatt S, et al. The impact of segmentation on whole-lung functional MRI quantification: Repeatability and reproducibility from multiple human observers and an artificial neural network. Magn Reson Med 2021;85(2):1079-1092. https://doi.org/10.1002/mrm.28476.

164. Astley JR, Biancardi AM, Hughes PJC, et al. Large-scale investigation of deep learning approaches for ventilated lung segmentation using multi-nuclear hyperpolarized gas MRI. Sci Rep 2022;12(1):10566. https://doi.org/10.1038/s41598-022-14672-2.

165. Capaldi DPI, Guo F, Xing L, Parraga G. Pulmonary ventilation maps generated with free-breathing proton MRI and a deep convolutional neural network. Radiology 2021;298(2):427-438. https://doi.org/10.1148/radiol.2020202861.

166. Schalekamp S, Klein WM, van Leeuwen KG. Current and emerging artificial intelligence applications in chest imaging: A pediatric perspective. Pediatr Radiol 2022;52(11):2120-2130. https://doi.org/10.1007/s00247-021-05146-0.

167. Ciet P, Eade C, Ho ML, et al. The unintended consequences of artificial intelligence in paediatric radiology. Pediatr Radiol 2024;54(4):585-593. https://doi.org/10.1007/s00247-023-05746-y.

168. Klimeš F, Voskrebenzev A, Wacker F, Vogel-Claussen J. Three-dimensional phase resolved functional lung magnetic resonance imaging. J Vis Exp 2024;208:e66385. https://doi.org/10.3791/66385.

169. Stewart NJ, Norquay G, Griffiths PD, Wild JM. Feasibility of human lung ventilation imaging using highly polarized naturally abundant xenon and optimized three-dimensional steady-state free precession. Magn Reson Med 2015;74(2):346-352. https://doi.org/10.1002/mrm.25732.

170. Bdaiwi AS, Svoboda AM, Murdock KE, et al. Quantifying abnormal alveolar microstructure in cystic fibrosis lung disease via hyperpolarized 129Xe diffusion MRI. J Cyst Fibros 2024;23:926-935. https://doi.org/10.1016/j.jcf.2024.07.002.